

Combination of terminal sliding mode and finite-time state-dependent Riccati equation: Flapping-wing flying robot control

Saeed Rafee Nekoo, José Ángel Acosta, and Anibal Ollero
GRVC Robotics Lab., Departamento de Ingeniería de Sistemas y Automática, Escuela Técnica Superior de Ingeniería, Universidad de Sevilla, Seville, Spain
saerafee@yahoo.com, (jaar, aollero)@us.es

Abstract

A novel terminal sliding mode control (TSMC) is introduced to control a class of nonlinear uncertain systems in finite-time. Having command on the definition of the final time as an input control parameter is the goal of this work. TSMC is naturally a finite time controller though the time cannot be set as input, and the convergence time is not exactly known to the user before execution of the control loop. The sliding surface of the introduced controller is equipped with a finite-time gain that finishes the control task in the desired predefined time. The gain is found by partitioning the state-dependent differential Riccati equation (SDDRE) gain, then arranging the sub-blocks in a symmetric positive-definite structure. The SDDRE is a nonlinear optimal controller with a final boundary condition that penalizes the states at the final time. This guides the states to the desired condition by imposing extra force on the input control law. Here the gain is removed from standard SDDRE control law (partitioned and made symmetric positive-definite) and inserted into the nonlinear sliding surface to present a novel finite-time TSMC. The stability of the proposed TSMC is guaranteed by the definition of the adaptive gain of TSMC, which is limited by the Lyapunov stability condition. The proposed approach was validated and compared with SDDRE and conventional TSMC as independent controllers, applied on a Van der Pole oscillator. The capability of the proposed approach of controlling complex systems was checked by simulating a flapping-wing flying robot (FWFR). The FWFR possesses a highly nonlinear model with uncertainty and disturbance caused by flapping. The flight assumptions also limit the input law significantly. The proposed TSMC successfully controlled the illustrative example and FWFR model and has been compared with SDDRE and conventional TSMC.

Keywords: Terminal sliding mode control; SDRE; Optimal control; Nonlinear control; Unmanned aerial vehicle.

1. Introduction

The sliding mode control (SMC) and variable structure systems are among the most popular nonlinear robust methods; they find the control law by defining a proper sliding surface. The SMC has so many branches such as a second-order, adaptive, terminal, and also in combination with other techniques including fuzzy, neural-network, optimal, optimal-integral, etc. [1]. The focus of this current research is on terminal sliding mode control (TSMC). The TSMC is an updated structure of the SMC, introduced in the 90s [2]. The terminal attractors in the new controller guarantee the finite-time state convergence. The nonlinear definition of the sliding surface makes the manifold an attractor [3]. Yu et al. used a continuous TSMC for controlling rigid robotic manipulators [4]. The TSMC was improved in many aspects: a nonsingular version of the controller [5, 6], fast terminal sliding mode control [7], fractional-order one [8], adaptive nonsingular [9], etc. Wang and Xu investigated the micro-positioning control system via an adaptive terminal sliding mode control [10]. The micro-positioning system used piezoelectric actuators that had resonance; the adaptive novel gain controlled the uncertain system with high performance. Xiong and Zhang employed global fast TSMC for quadrotor control in set-point regulation [11]. The system was divided into two fully- and under-actuated system and controlled successfully.

This current work intends to find a finite-time controller with robust characteristics. The TSMC is a good selection though the final time cannot be set as a control input parameter [12]. Shiri et al. solved the problem by dividing the sliding surface into two linear (conventional SMC) and nonlinear sections (nonsingular TSMC) [12]. Then it was possible to define the final time as an input to the control system. The controller was applied for a Van der Pole oscillator and a robotic manipulator. Here in this current work, the time setting approach is used and the final time could be defined as an input to the control system. On the contrary to Ref. [12], here in this work, one nonlinear sliding surface is considered. To have a command over the final time, an optimal gain of the state-dependent differential Riccati equation (SDDRE) is used. The SDDRE is a nonlinear closed-loop suboptimal controller with the power of finite-time control by penalizing a terminal boundary condition [13, 14]. Tripathy used the state-dependent differential Riccati equation for manipulator control [15]. There are several solution methods

to the differential Riccati equation such as backward integration [16], Lyapunov-based method [17, 18], and state transition matrix approach [19]. Here we used the Lyapunov-based approach as the solution to the SDDRE with negative gain. The gain of the SDDRE could be partitioned and used in other controllers preserving the finite-time characteristics.

Recently, the flapping-wing flying robot (FWFR) has been a challenging model for the assessment of the controllers in terms of robustness and performance. The model is highly nonlinear and coupled with force/moment components. One of the open problems in this field is the dynamic modeling of a flapping wing system. The six-degree-of-freedom (DoF) in modeling leads to complicated systems especially in terms of lift, drag, and aerodynamics calculations. The modeling of aircraft (Refs. [20, 21]) is the base of the modeling though the flapping wing adds complexity and changes to the system. The dynamic derivation of the gliding phase of the flapping systems is very similar to aircraft dynamic; however, the inertia and weight, and propulsion forces are significantly lower. The investigation began by looking into the bird's flight dynamics [22, 23]. Taylor and Thomas studied the flapping flight dynamics, longitudinal stability of animal flights [22]. Deng et al. researched flapping flight dynamics for insect-sized systems; studied the lift, drag, and body dynamic [24]. Platzer et al. reviewed the progress and challenges of flapping-wing flight considering different wing configurations [25]. It was found that thrust, lift, and propulsive efficiency on flapping mode depend on the frequency and amplitude of the flapping. The insect-sized flapping-wing systems have been attractive since the actuation of them and the weight of the system provided the flight situation more comfortable than large-scale flapping systems [26-33]. In that case, significant load-carrying capacity is not expected.

Increasing the size of the flapping-wing flying robot requires a complicated mechanical mechanism to obtain constant flapping and control over the frequency. Armanini et al. used flight data of experiments to define ornithopter dynamics through global system identification [34]. Hassan and Taha showed that the flight path of the flapping robot was subjected to vibration [35]. This result was found by relaxing the common assumption that neglected the wing inertial effects and directly averaged the dynamics over the flapping cycle. Bakhtiari et al. studied the modeling focusing on the aerodynamics effects on the edge of the tail, experimentally [36]. All the dynamics modeling (some works with the experimental investigation on lift, drag, and aerodynamics) and control implementations (mostly in theoretical schemes and simulations) lead the researchers towards carrying more weight to

apply the FWFR for a particular task [37-40]. One application is perception and visual inspection by FWFR which requires more lift capacity due to necessary external devices such as a camera, digital board, and heavier batteries [39]. The majority of the modeling used general dynamic modeling of a rigid body in gliding conditions with added lift, drag, and aerodynamics forces. The representations of the rigid body were similar though the aerodynamics modeling was different based on the situation and condition. In this work, six-DoF modeling of the FWFR using rigid body dynamics is considered. The aerodynamics of the system is added to the dynamic equation and the relation between the force/moment inputs and rudders and thrust actuators is presented using Taylor series expansion (linearized model). It should be emphasized that the model is nonlinear and coupled and the relation between force/moment and actuators is only linearized.

The main contributions:

- C1. Introducing a terminal sliding mode to control a class of nonlinear uncertain systems in predefined finite-time; that is defined as an input parameter.
- C2. Stability proof of the TSMC gain for a predefined finite-time control using the partitioned SDDRE control gain.
- C3. Six-DoF fully-actuated SDDRE-based TSMC control of FWFR (modeling and simulation).

The rest of the paper follows: Section 2 expresses the control structure of the proposed TSMC. Dynamic modeling of the FWFR is expressed in Section 3. State-space form and control implementation are reported in Section 4. Section 5 presents simulations: illustrative example, FWFR, and comparison with conventional SDDRE and TSMC. Concluding remarks are reported in Section 6.

Notations: \mathbb{R}^n denotes the n -dimensional Euclidean space; $\mathbb{R}^{n \times m}$ is the set of $m \times n$ real matrices; $(\cdot)^T$ is the transpose of a matrix or a vector; $\text{diag}(\cdot)$ means a diagonal matrix; $\mathbf{I}_{n \times n}$ and $\mathbf{0}_{n \times n}$ denote $n \times n$ identity and zero matrices. $|\cdot|$ defines absolute value and $\|\cdot\|_2$ is norm-2 of a vector or a matrix. $\text{eig}[\mathbf{A}]$ provides a diagonal matrix with eigenvalues of \mathbf{A} .

2. Terminal Sliding Mode Control

2-1. System Definition

Consider a second-order nonlinear differential equation

$$\ddot{\mathbf{q}} = \mathbf{f}(\mathbf{q}, \dot{\mathbf{q}}) + \mathbf{E}(\mathbf{q})\mathbf{u} + \Psi(\mathbf{q}, \dot{\mathbf{q}}, t), \quad (1)$$

subjected to unknown external disturbance $\Psi(\mathbf{q}, \dot{\mathbf{q}}, t): \mathbb{R}^n \times \mathbb{R}^n \times \mathbb{R}^+ \rightarrow \mathbb{R}^n$, which is bounded $\Psi(\mathbf{q}, \dot{\mathbf{q}}, t) \leq \Psi_c(\mathbf{q}, \dot{\mathbf{q}}, t)$. Equation (1) presents a fully actuated mechanical system. The generalized coordinates of system (1) are collected in $\mathbf{q} \in \mathbb{R}^n$ vector and the input force or torque in $\mathbf{u} \in \mathbb{R}^n$ in which n denotes the degree-of-freedom (DoF). The system is limited to a common form that covers a wide range of mechanical systems by defining $\mathbf{f}(\mathbf{q}, \dot{\mathbf{q}}) = -\mathbf{M}^{-1}(\mathbf{q})(\mathbf{c}(\mathbf{q}, \dot{\mathbf{q}}) + \mathbf{g}(\mathbf{q}) + \mathbf{D}(\mathbf{q}, \dot{\mathbf{q}})\dot{\mathbf{q}})$ and $\mathbf{E}(\mathbf{q}) = \mathbf{M}^{-1}(\mathbf{q})$ where $\mathbf{M}(\mathbf{q}): \mathbb{R}^n \rightarrow \mathbb{R}^{n \times n}$ is inertia matrix, $\mathbf{c}(\mathbf{q}, \dot{\mathbf{q}}): \mathbb{R}^n \times \mathbb{R}^n \rightarrow \mathbb{R}^n$ is Coriolis and centrifugal vector, $\mathbf{g}(\mathbf{q}): \mathbb{R}^n \rightarrow \mathbb{R}^n$ is a vector that includes gravity terms, $\mathbf{D}(\mathbf{q}, \dot{\mathbf{q}}): \mathbb{R}^n \times \mathbb{R}^n \rightarrow \mathbb{R}^{n \times n}$ collects all terms related to friction, drag (underwater or flying systems), aerodynamics forces, etc.

Selecting the state vector as $\mathbf{x}_{2n \times 1} = [\mathbf{q}^T, \dot{\mathbf{q}}^T]^T$, the reduced-order differential equation (state-space representation of (1)) is found:

$$\dot{\mathbf{x}} = \mathbf{a}(\mathbf{x}) + \mathbf{g}(\mathbf{x}, \mathbf{u}) = \begin{bmatrix} \dot{\mathbf{q}} \\ \mathbf{f}(\mathbf{q}, \dot{\mathbf{q}}) \end{bmatrix} + \begin{bmatrix} \mathbf{0}_{n \times n} \\ \mathbf{E}(\mathbf{q}) \end{bmatrix} \mathbf{u} + \begin{bmatrix} \mathbf{0}_{n \times 1} \\ \Psi(\mathbf{q}, \dot{\mathbf{q}}, t) \end{bmatrix}, \quad (2)$$

where $\mathbf{a}(\mathbf{x}): \mathbb{R}^{2n} \rightarrow \mathbb{R}^{2n}$ and $\mathbf{g}(\mathbf{x}, \mathbf{u}): \mathbb{R}^{2n} \times \mathbb{R}^n \rightarrow \mathbb{R}^{2n}$ are piecewise-continuous vector-valued functions that satisfy the Lipschitz condition.

2-2. The Symmetric Gain of State-dependent Riccati Equation

In this section, the finite-time suboptimal gain of the SDRE will be partitioned into four square blocks and will be used in the definition of the sliding surface in Section 2-3. The SDRE control law will not be used directly; however, the finite-time gain will be used in the definition of the TSMC sliding surface. The first step is to rewrite state-space representation (2) in the state-dependent coefficient (SDC) parameterization:

$$\dot{\mathbf{x}} = \mathbf{A}(\mathbf{x})\mathbf{x} + \mathbf{B}(\mathbf{x})\mathbf{u} = \begin{bmatrix} \mathbf{0}_{n \times n} & | & \mathbf{I}_{n \times n} \\ \hline \mathbf{0}_{n \times n} & | & -\mathbf{M}^{-1}(\mathbf{q})(\mathbf{C}(\mathbf{q}, \dot{\mathbf{q}}) + \mathbf{D}(\mathbf{q}, \dot{\mathbf{q}})) \end{bmatrix} \mathbf{x} + \begin{bmatrix} \mathbf{0}_{n \times n} \\ \mathbf{E}(\mathbf{q}) \end{bmatrix} \mathbf{u}, \quad (3)$$

where $\mathbf{A}(\mathbf{x}): \mathbb{R}^{2n} \rightarrow \mathbb{R}^{2n \times 2n}$, $\mathbf{B}(\mathbf{x}): \mathbb{R}^{2n} \rightarrow \mathbb{R}^{2n \times n}$ and $\mathbf{c}(\mathbf{q}, \dot{\mathbf{q}}) = \mathbf{C}(\mathbf{q}, \dot{\mathbf{q}})\dot{\mathbf{q}}$.

Remark 1. The gravity vector usually contains trigonometric functions (robotic arms) or constant values (flying objects). The $\cos(\cdot)$ function cannot be factored after using Taylor series expansion since the first term is 1. Also dividing $\frac{\cos(\cdot)}{x_i}$ imposes singularities at equilibrium $x_i = 0$. So, the gravity vector will be

removed from SDC matrices (3), and will be compensated in TSMC control law.

Condition 1. $\{\mathbf{A}(\mathbf{x}), \mathbf{B}(\mathbf{x})\}$ is a completely controllable parameterization of system (2) for all \mathbf{x} in $t \in [0, t_f]$ [41].

Property 1. $\mathbf{M}(\mathbf{q})$ is a symmetric positive-definite matrix such that $\mathbf{M}_1 \leq \mathbf{M}(\mathbf{q}(t)) \leq \mathbf{M}_2$ where $\mathbf{M}_1, \mathbf{M}_2 \in \mathbb{R}^{n \times n}$ are constant symmetric positive definite matrices.

Remark 2. Concerning Property 1, the diagonal elements of $\mathbf{E}(\mathbf{q})$ are always positive even at $\mathbf{q} = \mathbf{0}$. The pair of $\mathbf{A}(\mathbf{0})$ and $\mathbf{B}(\mathbf{0})$ is completely controllable and in the rest of the domain, the worst-case scenario is the pair of $\begin{bmatrix} \mathbf{0} & \mathbf{I} \\ \mathbf{0} & -\mathbf{E}(\mathbf{0})\mathbf{D} \end{bmatrix}$ and $\begin{bmatrix} \mathbf{0} \\ \mathbf{E}(\mathbf{0}) \end{bmatrix}$. It is clear that the case of $\begin{bmatrix} \mathbf{0} & \mathbf{I} \\ \mathbf{0} & \mathbf{0} \end{bmatrix}$ and $\begin{bmatrix} \mathbf{0} \\ \mathbf{I} \end{bmatrix}$ is controllable. So, the SDC pair in (3), presents a completely controllable parameterization.

The cost function is:

$$J = \frac{1}{2} \left(\int_0^{t_f} [\mathbf{u}^T \mathbf{R}(\mathbf{x}) \mathbf{u} + \mathbf{x}^T \mathbf{Q}(\mathbf{x}) \mathbf{x}] dt + \mathbf{x}^T(t_f) \mathbf{F} \mathbf{x}(t_f) \right), \quad (4)$$

where $\mathbf{R}(\mathbf{x}): \mathbb{R}^{2n} \rightarrow \mathbb{R}^{n \times n}$ is input weighting matrix, symmetric positive-definite, and $\mathbf{Q}(\mathbf{x}): \mathbb{R}^{2n} \rightarrow \mathbb{R}^{2n \times 2n}$ is state weighting matrix, symmetric positive-semi-definite. $\mathbf{F} \in \mathbb{R}^{2n \times 2n}$ also penalizes the states at the terminal time t_f ; $\mathbf{F} = \mathbf{F}^T$ and $\mathbf{F} \geq \mathbf{0}$.

Condition 2. $\{\mathbf{A}(\mathbf{x}), \mathbf{Q}^{\frac{1}{2}}(\mathbf{x})\}$, in (4), is a completely observable parameterization of system (2) for all \mathbf{x} in $t \in [0, t_f]$, where $\mathbf{Q}^{1/2}(\mathbf{x})$ is Cholesky decomposition of $\mathbf{Q}(\mathbf{x})$ [41].

Defining all matrices, $\mathbf{A}(\mathbf{x})$, $\mathbf{B}(\mathbf{x})$, $\mathbf{Q}(\mathbf{x})$, $\mathbf{R}(\mathbf{x})$ and \mathbf{F} , one could solve the state-dependent differential Riccati equation:

$$-\dot{\mathbf{K}}(\mathbf{x}) = \mathbf{A}^T(\mathbf{x})\mathbf{K}(\mathbf{x}) + \mathbf{K}(\mathbf{x})\mathbf{A}(\mathbf{x}) + \mathbf{Q}(\mathbf{x}) - \mathbf{K}(\mathbf{x})\mathbf{B}(\mathbf{x})\mathbf{R}^{-1}(\mathbf{x})\mathbf{B}^T(\mathbf{x})\mathbf{K}(\mathbf{x}), \quad (5)$$

with terminal boundary condition $\mathbf{K}(\mathbf{x}(t_f)) = \mathbf{F}$.

Lemma 1. The nonlinear system (3), with SDC pair based on Conditions 1 and 2, can be stabilized using the standard SDDRE control law $\mathbf{u} = -\mathbf{R}^{-1}(\mathbf{x})\mathbf{B}^T(\mathbf{x})\mathbf{K}(\mathbf{x})\mathbf{x}$, in which $\mathbf{K}(\mathbf{x})$ is symmetric positive-definite solution to SDDRE (5) [42].

The proof of Lemma 1 could be found by using the Lyapunov candidate $V(\mathbf{x}) = \mathbf{x}^T \mathbf{K}(\mathbf{x}) \mathbf{x}$. The details of solution methods to (5) could be visited in Ref. [42]; we suppose that

SDDRE could be solved with one of the methods such as the Lyapunov-based approach with negative gain.

The control gain, the solution to the SDDRE, is partitioned into four-square blocks [43]:

$$\mathbf{K}(\mathbf{x}) = \begin{bmatrix} \mathbf{K}_{11}(\mathbf{x}) & \mathbf{K}_{12}(\mathbf{x}) \\ \mathbf{K}_{12}^T(\mathbf{x}) & \mathbf{K}_{22}(\mathbf{x}) \end{bmatrix}_{2n \times 2n},$$

and is substituted in overall control gain

$$\mathbf{X}(\mathbf{x}) = \mathbf{R}^{-1}(\mathbf{x})\mathbf{B}^T(\mathbf{x})\mathbf{K}(\mathbf{x}) = [\mathbf{X}_1(\mathbf{x}) \quad \mathbf{X}_2(\mathbf{x})]_{n \times 2n},$$

in which

$$\mathbf{X}_1(\mathbf{x}) = \mathbf{R}^{-1}(\mathbf{x})\mathbf{M}^{-1}(\mathbf{q})\mathbf{K}_{12}^T(\mathbf{x}),$$

$$\mathbf{X}_2(\mathbf{x}) = \mathbf{R}^{-1}(\mathbf{x})\mathbf{M}^{-1}(\mathbf{q})\mathbf{K}_{22}(\mathbf{x}).$$

The gain $\mathbf{X}_1(\mathbf{x})$ is multiplied by the position vector, $\mathbf{q}(t)$, and $\mathbf{X}_2(\mathbf{x})$ by the velocity vector, $\dot{\mathbf{q}}(t)$. From a general point of view $\mathbf{X}_1(\mathbf{x})$ acts as proportional gain and $\mathbf{X}_2(\mathbf{x})$ as a derivative one.

Remark 3. The proportional and derivative gains $\mathbf{X}_1(\mathbf{x})$ and $\mathbf{X}_2(\mathbf{x})$ possess finite-time characteristics for the regulation of the error and velocity of the error vector to zero, tuned by \mathbf{F} .

The finite-time proportional gain of the SDDRE is required for the definition of the sliding surface in Section 2-3, though it is not a symmetric positive definite gain. To define the gain in that shape, and preserve the finite time characteristics, it will be transformed into [43]:

$$\mathbf{K}_{SP}(\mathbf{x}) = \frac{\mathbf{K}_{12}(\mathbf{x})\mathbf{M}^{-1}(\mathbf{x})\mathbf{R}^{-1}(\mathbf{x})\mathbf{M}^{-1}(\mathbf{x})\mathbf{K}_{12}^T(\mathbf{x})}{\|\mathbf{K}_{12}(\mathbf{x})\mathbf{M}^{-1}(\mathbf{x})\|_2}, \quad (6)$$

where $\mathbf{K}_{SP}(\mathbf{x})$ is made symmetric by multiplication of $\mathbf{K}_{12}(\mathbf{x})\mathbf{M}^{-1}(\mathbf{x})$ from the left-hand side of the equation and leveled by division to the norm-2 of that $\|\mathbf{K}_{12}(\mathbf{x})\mathbf{M}^{-1}(\mathbf{x})\|_2$.

If the weighting matrix of states (preserving symmetric positive-definite condition) at final time is partitioned into four submatrices:

$$\mathbf{F} = \begin{bmatrix} \mathbf{F}_{11} & \mathbf{F}_{12} \\ \mathbf{F}_{12}^T & \mathbf{F}_{22} \end{bmatrix}, \quad (7)$$

then, the \mathbf{F}_{12} sub-block will define the final boundary condition of $\mathbf{K}_{12}(\mathbf{x})$ in (6), as $\mathbf{K}_{12}(t_f) = \mathbf{F}_{12}$. However, \mathbf{F}_{12} is sign-indefinite and for bounding $\mathbf{K}_{SP}(\mathbf{x})$ in Section 2-3, a positive definite \mathbf{F}_{12} is required. As a result, the following conditions are considered: \mathbf{F}_{11} , \mathbf{F}_{12} , and \mathbf{F}_{22} are diagonal matrices with positive components, and $\mathbf{F}_{12} < \sqrt{\mathbf{F}_{11}\mathbf{F}_{22}}$. This provides a positive definite symmetric \mathbf{F} and also \mathbf{F}_{12} .

Assumption 1. It is assumed that \mathbf{F}_{11} , \mathbf{F}_{12} , and \mathbf{F}_{22} , in Eq. (7), are diagonal matrices with positive components, and $\mathbf{F}_{12} < \sqrt{\mathbf{F}_{11}\mathbf{F}_{22}}$, then it is also assumed that $\text{eig}[\mathbf{K}_{\text{SP}}(\mathbf{x})] \leq \mathbf{F}_{12}$ for all $\mathbf{x} \in \mathbb{R}^{2n}$ in $t \in [0, t_f]$.

Assumption 1 implies that the final weighting matrix must be chosen relatively bigger than the weighting matrix of states, $\mathbf{F} \gg \mathbf{Q}(\mathbf{x})$, or in other words, $\mathbf{F}_{12} \gg [\mathbf{Q}_{12}(\mathbf{x})]_{n \times n}$ to force the solution to start from an initial condition and move to a large final boundary condition.

2-3. The SDRE-TSMC Design

Consider the state-space representation of the general nonlinear affine-in-control time-invariant system (2). The goal is to define a robust nonlinear control law to regulate the error of the system to the desired condition in predefined terminal time. The terminal sliding mode is a finite-time controller in nature though the user cannot set the final time as an input to the control problem using common standard forms. The terminal sliding mode controller is finite time in nature; however, the final time cannot be introduced as an input to the control system. The reason is that the total final time is the summation of rise time and settling time, $t_f = t_r + t_s$. Calculation of t_s needs the computation of $e(t_r)$, and this value (error at rise time) is unknown before simulation of the system or implementation of the experiment. So, while the terminal time is finite, the user does not know the exact final time before the implementation. Shiri et al. used two sliding surfaces to present a structure accepting the final time as an input to a nonsingular terminal sliding mode controller [12]. A linear sliding surface was responsible to define the reaching time and the nonlinear one set the convergence time; together they could determine the total final time. The combination of terminal sliding mode and finite-time state-dependent Riccati equation provides a solution for determining the final time before implementation of the controller and forces the system to finish its control task by weighting matrices of the SDRE. Here, one nonlinear sliding surface is selected with a finite-time gain to present a simpler structure.

The nonlinear sliding surface is designed as

$$s_i = \dot{e}_i + \beta \text{sign} \left(\sum_{j=1}^n K_{\text{SP},ij}(\mathbf{x}) e_j \right) \left| \sum_{j=1}^n K_{\text{SP},ij}(\mathbf{x}) e_j \right|^{\frac{q}{p}}, \quad (8)$$

for $i = 1, \dots, n$; $\beta > 0$, q and p are positive odd integers following $p > q$. $\sum_{j=1}^n K_{\text{SP},ij}(\mathbf{x})$ denotes the i -th row of proportional SDDRE gain $\mathbf{K}_{\text{SP}}(\mathbf{x})$.

Remark 4. The definition of the sliding surface uses the relative part to position variables of the system in regulation, $\mathbf{K}_{SP}(\mathbf{x})$. Observing the selection weighting matrices for the SDRE in the literature [42, 44-46], it can be seen that for precise and fast position control using optimal control, the velocity states must be relaxed. So, the role of the proportional gain is more highlighted. To keep the focus on position states and also present a sliding surface as simple as possible, the control gain related to derivative states, $\mathbf{X}_2(\mathbf{x})$, is not included in Eq. (8).

The error vector is defined as $\mathbf{e}(t) = \mathbf{q}(t) - \mathbf{q}_{des}(t)$ in which $\mathbf{q}_{des}(t) \in \mathbb{R}^n$ is the desired values for the generalized coordinates. Derivation of the error also results in $\dot{\mathbf{e}}(t) = \dot{\mathbf{q}}(t) - \dot{\mathbf{q}}_{des}(t)$ in trajectory tracking and $\dot{\mathbf{e}}(t) = \dot{\mathbf{q}}(t)$ in regulation; and:

$$\ddot{\mathbf{e}}(t) = \ddot{\mathbf{q}}(t) - \ddot{\mathbf{q}}_{des}(t) = \mathbf{f}(\mathbf{q}, \dot{\mathbf{q}}) + \mathbf{E}(\mathbf{q})\mathbf{u} + \Psi(\mathbf{q}, \dot{\mathbf{q}}, t) - \ddot{\mathbf{q}}_{des}(t). \quad (9)$$

Assumption 2. The unknown system is bounded above, the vector $f_i(\mathbf{x}) \leq \hat{f}_i(\mathbf{x})$ and matrix $\sum_{i=1}^n \sum_{j=1}^n E_{ij}(\mathbf{x}) \leq \sum_{i=1}^n \sum_{j=1}^n \hat{E}_{ij}(\mathbf{x})$ to the values $\hat{f}_i(\mathbf{x})$ and $\hat{E}_{ij}(\mathbf{x})$.

Assumption 3. The deviation of the external disturbance, $\mathbf{f}(\mathbf{x})$ and $\mathbf{E}(\mathbf{x})$ from their bounds are limited to the known values:

$$|\max(\Psi(\mathbf{x}, t)) - \mathbf{E}(\mathbf{x})\hat{\mathbf{E}}^{-1}(\mathbf{x}) \max(\Psi_c(\mathbf{x}, t))| \leq \Psi_0(\mathbf{x}), \quad (10)$$

$$|\mathbf{f}(\mathbf{x}) - \mathbf{E}(\mathbf{x})\hat{\mathbf{E}}^{-1}(\mathbf{x})\hat{\mathbf{f}}(\mathbf{x})| \leq \mathbf{f}_0(\mathbf{x}), \quad (11)$$

$$\mathbf{E}_{\min}(\mathbf{x}) \leq \mathbf{E}(\mathbf{x})\hat{\mathbf{E}}^{-1}(\mathbf{x}) \leq \mathbf{E}_{\max}(\mathbf{x}). \quad (12)$$

The convergence and stability of the TSMC have two parts, stage 1, showing the convergence of the system to the sliding surface, and stage 2, the convergence of the error to zero on the sliding surface [5, 47]. The latter is done by computation of the settling time on the sliding surface $\mathbf{s} = \mathbf{0}$. The both steps could be expressed in one theorem such as Refs. [5, 47]; however, for simplification in finite time calculation, we presented it in two Theorems 1 and 2. The stability discussion of the proposed TSMC is studied by following steps: First, the convergence of the system to the sliding surface in reaching time, t_r , will be shown and proved, Theorem 1. Then the computation of the reaching time is presented in Lemma 2. Finally, the convergence of the error (along with the sliding surface $\mathbf{s} = \mathbf{0}$) to zero in finite time will be shown by computation of the final time, $T = t_r + t_s$, where t_s is the settling time, Theorem 2.

Theorem 1. (Convergence to the sliding surface). Considering Assumptions 2 and 3, the nonlinear system (2) will reach the sliding surface (8), $\mathbf{s} = \mathbf{0}$, in t_r by control law $\mathbf{u} = \hat{\mathbf{E}}^{-1}(\mathbf{x}) \left(\ddot{\mathbf{q}}_{\text{des}} - \hat{\mathbf{f}}(\mathbf{x}) - \beta \frac{q}{p} \mathbf{e}_s \right) - \mathbf{K}_T(\mathbf{x}) \text{sign}(\mathbf{s})$, where $\mathbf{K}_T(\mathbf{x}) \geq \text{diag}(|\mathbf{E}(\mathbf{x})|^{-1}(\boldsymbol{\eta} + |\boldsymbol{\Gamma}(\mathbf{x})|))$ in which $\boldsymbol{\eta} \in \mathbb{R}^n$, $\boldsymbol{\eta} > \mathbf{0}$ and $\boldsymbol{\Gamma}(\mathbf{x})$ and \mathbf{e}_s are set along with the proof.

Proof. A Lyapunov candidate is used $V = \frac{1}{2} \mathbf{s}^T \mathbf{s}$ to guarantee stability through its derivative $\dot{V} = \mathbf{s}^T \dot{\mathbf{s}} < -\boldsymbol{\eta}^T |\mathbf{s}|$, known as the sliding condition. The derivative of the sliding surface (8) should be computed (please see the details in Appendix 1):

$$\dot{s}_i = \ddot{e}_i + \beta \frac{q}{p} \left[\sum_{j=1}^n \dot{K}_{\text{SP},ij}(\mathbf{x}) e_j + K_{\text{SP},ij}(\mathbf{x}) \dot{e}_j \right] \left| \sum_{j=1}^n K_{\text{SP},ij}(\mathbf{x}) e_j \right|^{\frac{q}{p}-1}, \quad (13)$$

to form the condition $\dot{s}_i = 0$, for providing the equivalent control part. Substituting \ddot{e}_i , Eq. (9), in (13) and mathematical manipulation, one could present

$$\begin{aligned} & \sum_{j=1}^n (\hat{E}_{ij}(\mathbf{x}) u_{n,j}) \\ &= \ddot{q}_{\text{des},i} - \hat{f}_i(\mathbf{x}) - \Psi_{c,i}(\mathbf{x}, t) \\ & - \beta \frac{q}{p} \left[\sum_{j=1}^n \dot{K}_{\text{SP},ij}(\mathbf{x}) e_j + K_{\text{SP},ij}(\mathbf{x}) \dot{e}_j \right] \left| \sum_{j=1}^n K_{\text{SP},ij}(\mathbf{x}) e_j \right|^{\frac{q}{p}-1}, \end{aligned} \quad (14)$$

in which $\ddot{q}_i = \hat{f}_i(\mathbf{x}) + \sum_{j=1}^n (\hat{E}_{ij}(\mathbf{x}) u_{n,j})$ is replaced with the upper bounds of the system dynamics, Assumption 2, $f_i(\mathbf{x}) \leq \hat{f}_i(\mathbf{x})$ and $\sum_{i=1}^n \sum_{j=1}^n E_{ij}(\mathbf{x}) \leq \sum_{i=1}^n \sum_{j=1}^n \hat{E}_{ij}(\mathbf{x})$ where $u_{n,j}$ is j -th equivalent control signal, and $\Psi_{c,i}(\mathbf{x}, t)$ which is the upper bound of $\Psi_i(\mathbf{x}, t)$. Expressing the matrix/vector presentation of (14), the equivalent or nominal control is presented:

$$\mathbf{u}_n = \hat{\mathbf{E}}^{-1}(\mathbf{x}) \left(\ddot{\mathbf{q}}_{\text{des}} - \hat{\mathbf{f}}(\mathbf{x}) - \boldsymbol{\Psi}_c(\mathbf{x}, t) - \beta \frac{q}{p} \mathbf{e}_s \right), \quad (15)$$

where

$$\mathbf{e}_s := \begin{bmatrix} \left[\sum_{j=1}^n \dot{K}_{SP,1j}(\mathbf{x})e_j + K_{SP,1j}(\mathbf{x})\dot{e}_j \right] \left| \sum_{j=1}^n K_{SP,1j}(\mathbf{x})e_j \right|^{\frac{q}{p}-1} \\ \vdots \\ \left[\sum_{j=1}^n \dot{K}_{SP,nj}(\mathbf{x})e_j + K_{SP,nj}(\mathbf{x})\dot{e}_j \right] \left| \sum_{j=1}^n K_{SP,nj}(\mathbf{x})e_j \right|^{\frac{q}{p}-1} \end{bmatrix}. \quad (16)$$

A correction part will be added to the nominal control (15) to complete the TSMC input law:

$$\mathbf{u} = \mathbf{u}_n + \mathbf{u}_{\text{corr}} = \hat{\mathbf{E}}^{-1}(\mathbf{x}) \left(\ddot{\mathbf{q}}_{\text{des}} - \hat{\mathbf{f}}(\mathbf{x}) - \Psi_c(\mathbf{x}, t) - \beta \frac{q}{p} \mathbf{e}_s \right) - \mathbf{K}_T(\mathbf{x}) \text{sign}(\mathbf{s}). \quad (17)$$

The gain $\mathbf{K}_T(\mathbf{x}): \mathbb{R}^{2n} \rightarrow \mathbb{R}^{n \times n}$ is determined by the sliding condition $\mathbf{s}^T \dot{\mathbf{s}} < -\boldsymbol{\eta}^T |\mathbf{s}|$. Substituting the actual system (1) and control law (17) into sliding condition, it is rewritten as

$$\begin{aligned} \mathbf{s}^T \left(\mathbf{f}(\mathbf{x}) + \Psi(\mathbf{x}, t) - \mathbf{E}(\mathbf{x}) \hat{\mathbf{E}}^{-1}(\mathbf{x}) [\hat{\mathbf{f}}(\mathbf{x}) + \Psi_c(\mathbf{x}, t)] \right. \\ \left. - \left(\mathbf{I} - \mathbf{E}(\mathbf{x}) \hat{\mathbf{E}}^{-1}(\mathbf{x}) \right) \left(\ddot{\mathbf{q}}_{\text{des}} - \beta \frac{q}{p} \mathbf{e}_s \right) - \mathbf{E}(\mathbf{x}) \mathbf{K}_T(\mathbf{x}) \text{sign}(\mathbf{s}) \right) \\ < -\boldsymbol{\eta}^T |\mathbf{s}|. \end{aligned} \quad (18)$$

The sliding condition (18) is represented in compact form:

$$\mathbf{s}^T (\boldsymbol{\Gamma}(\mathbf{x}) - \boldsymbol{\delta}(\mathbf{x}) \text{sign}(\mathbf{s})) < -\boldsymbol{\eta}^T |\mathbf{s}|, \quad (19)$$

in which

$$\begin{aligned} \boldsymbol{\Gamma}(\mathbf{x}) &= \mathbf{f}(\mathbf{x}) + \Psi(\mathbf{x}, t) - \mathbf{E}(\mathbf{x}) \hat{\mathbf{E}}^{-1}(\mathbf{x}) [\hat{\mathbf{f}}(\mathbf{x}) + \Psi_c(\mathbf{x}, t)] \\ &\quad - \left(\mathbf{I} - \mathbf{E}(\mathbf{x}) \hat{\mathbf{E}}^{-1}(\mathbf{x}) \right) \left(\ddot{\mathbf{q}}_{\text{des}} - \beta \frac{q}{p} \mathbf{e}_s \right), \\ \boldsymbol{\delta}(\mathbf{x}) &= \mathbf{E}(\mathbf{x}) \mathbf{K}_T(\mathbf{x}). \end{aligned}$$

The scalar form of Eq. (19) is

$$\sum_{i=1}^n \left[s_i \left(\Gamma_i(\mathbf{x}) - \sum_{j=1}^n \delta_{ij}(\mathbf{x}) \text{sign}(s_j) \right) \right] \leq \sum_{i=1}^n -\eta_i |s_i|,$$

which can be represented as

$$\sum_{i=1}^n s_i \left(\sum_{j=1}^n \delta_{ij}(\mathbf{x}) \text{sign}(s_j) \right) \geq \sum_{i=1}^n \eta_i |s_i| + \sum_{i=1}^n s_i \Gamma_i(\mathbf{x}). \quad (20)$$

Dividing Eq. (20) by s_i removes i -summation

$$\sum_{j=1}^n \delta_{ij}(\mathbf{x}) \text{sign}(s_j) \geq \eta_i \frac{|s_i|}{\underbrace{s_i}_{\text{sign}(s_i)}} + \Gamma_i(\mathbf{x}),$$

then computing the absolute value of that results in

$$\begin{aligned} \left| \sum_{j=1}^n \delta_{ij}(\mathbf{x}) \text{sign}(s_j) \right| &\geq |\eta_i \text{sign}(s_i) + \Gamma_i(\mathbf{x})| \Rightarrow \left| \sum_{j=1}^n \delta_{ij}(\mathbf{x}) \right| |\text{sign}(s_j)| \\ &\geq |\eta_i| |\text{sign}(s_i)| + |\Gamma_i(\mathbf{x})|, \end{aligned}$$

which could define

$$\left| \sum_{j=1}^n \delta_{ij}(\mathbf{x}) \right| \geq \eta_i + |\Gamma_i(\mathbf{x})|. \quad (21)$$

Changing (21) to matrix form will obtain a vector

$$\bar{\mathbf{K}}_T(\mathbf{x}) \geq |\mathbf{E}(\mathbf{x})|^{-1} (\boldsymbol{\eta} + |\boldsymbol{\Gamma}(\mathbf{x})|). \quad (22)$$

Substituting $\boldsymbol{\Gamma}(\mathbf{x})$ in (22) and considering Assumption 3 result in inequality in terms of the defined bounds, using Eqs. (10)-(12):

$$\bar{\mathbf{K}}_T(\mathbf{x}) \geq |\mathbf{E}_{\min}(\mathbf{x}) \hat{\mathbf{E}}(\mathbf{x})|^{-1} \left(\boldsymbol{\eta} + \left| \mathbf{f}_0(\mathbf{x}) + \boldsymbol{\Psi}_0(\mathbf{x}) - (\mathbf{I} - \mathbf{E}_{\max}(\mathbf{x})) \left(\dot{\mathbf{q}}_{\text{des}} - \beta \frac{q}{p} \mathbf{e}_s \right) \right| \right),$$

which represents the diagonal arrays of $\mathbf{K}_T(\mathbf{x}) = \text{diag}(\bar{\mathbf{K}}_T(\mathbf{x}))$. Note that Eq. (12) results in $|\mathbf{E}_{\min}(\mathbf{x}) \hat{\mathbf{E}}(\mathbf{x})|^{-1} \geq |\mathbf{E}(\mathbf{x})|^{-1}$. ■

Remark 5. The term $|\mathbf{e}|^{\frac{q}{p}-1}$ in the conventional sliding surface is singular in regulation when $\lim_{\mathbf{e} \rightarrow 0} |\mathbf{e}|^{\frac{q}{p}-1} = \infty$ because of the negative power of error $\left(\frac{q}{p} - 1\right) < 0$.

Here in this work, the new form also faces singularity $|\mathbf{K}_{\text{SP}}(\mathbf{x}) \mathbf{e}|^{\frac{q}{p}-1}$ when $\lim_{\mathbf{e} \rightarrow 0} |\mathbf{K}_{\text{SP}}(\mathbf{x}) \mathbf{e}|^{\frac{q}{p}-1} = \infty$. Saturation bound of the inputs and the fact that in simulation and practice the error will not go to absolute zero provided the possibility of the presented results in Section 5.

Time analysis is a critical subject in terminal sliding mode control and computation of the settling time is done in the literature. The required time for the error, $\mathbf{e}(t)$, to move between the initial condition and the reaching point of the sliding surface is so-called reaching time, t_r ; and the remaining time for the error to converge from reaching time $\mathbf{e}(t_r)$ to equilibrium point

(with a specified error band) is so-called settling time t_s . The sum of reaching and settling time provide the necessary time for convergence of the TSMC $T = t_r + t_s$ (terminal time), see Fig. 1. In this work, the necessary time of convergence, T , is different from final time of operation, t_f . Here we define t_f as an input parameters; however, T might be bigger or less than that, and is known after the simulation or experiment based on the error value. Usually, the control designer prefers a faster final time.

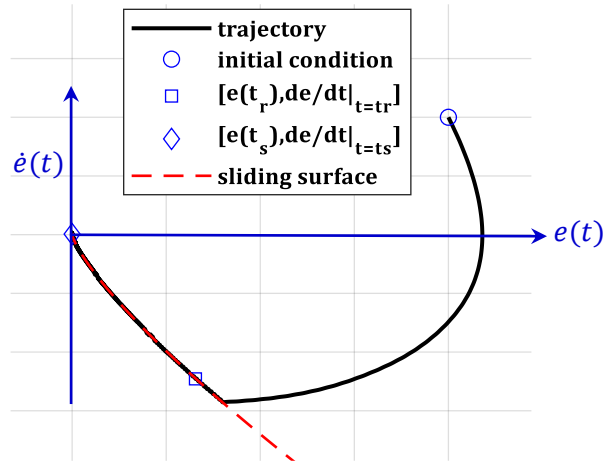


Fig. 1. Definition of the reaching and settling time of the terminal sliding surface.

Lemma 2. (*Reaching time* [48]) The reaching time of i -th error $e_i(t)$ to sliding surface is defined by $t_{r,i} \leq \frac{|s_i(0)|}{\eta_i}$.

Regarding the sliding condition in Theorem 1, the reaching time of i -th error in Lemma 2 is computed by integrating sliding condition $\frac{1}{2} \frac{d}{dt} s_i^2 < -\eta_i |s_i|$ between 0 and $t_{r,i}$:

$$\frac{1}{2} \int_{s_i(0)}^{s_i(t_{r,i})} \frac{ds_i^2}{\sqrt{s_i^2}} \leq -\eta_i \int_0^{t_{r,i}} dt \Rightarrow \underbrace{\sqrt{s_i^2(t_{r,i})}}_0 - \sqrt{s_i^2(0)} \leq -\eta_i t_{r,i} \Rightarrow t_{r,i} \leq \frac{|s_i(0)|}{\eta_i}.$$

Lemma 3. (*Settling time of conventional TSMC* [49]) The settling time of the conventional terminal sliding mode control is defined by $t_{s,i} = \frac{|e_i(t_{r,i})|^{1-\frac{q}{p}}}{\beta(1-\frac{q}{p})}$.

At reaching time, $t_{r,i}$, the sliding surface is zero which results in $\frac{de_i}{dt} = -\beta e_i |e_i|^{\frac{q}{p}-1}$, and after integration

$$-\frac{1}{\beta} \int_{e_i(t_{r,i})}^0 \frac{de_i}{e_i |e_i|^{\frac{q}{p}-1}} = -\frac{1}{\beta} \int_{e_i(t_{r,i})}^0 \frac{de_i}{e_i \left(\sqrt{e_i^2}\right)^{\frac{q}{p}-1}} = \int_{t_{r,i}}^{t_{s,i}+t_{r,i}} dt,$$

results in $t_{s,i} = \frac{|e_i(t_{r,i})|^{1-\frac{q}{p}}}{\beta(1-\frac{q}{p})}$ for conventional TSMC.

If the gain $\mathbf{K}_{SP}(\mathbf{x})$ is removed from sliding surface (8), the control structure will be similar to a conventional TSMC. So, the gain $\mathbf{K}_{SP}(\mathbf{x})$ manipulates the time in control structure. To compare the final time of the control problem with conventional TSMC, Lemma 3 has been expressed (in detail) for comparison.

Theorem 2. Considering Assumption 1, $\text{eig}[\mathbf{K}_{SP}(\mathbf{x}(t))] \leq \mathbf{F}_{12}$, the error of system (2), on the sliding surface, $\mathbf{s} = \mathbf{0}$, converges to zero in finite time T , defined by summation of reaching time, stated in Lemma 2 and upper bound of settling

$$\text{time, as } T = \max(t_{r,i} + t_{s,i}) \text{ in which } \begin{bmatrix} t_{s,1} \\ \vdots \\ t_{s,n} \end{bmatrix} \leq \frac{1}{\beta(1-\frac{q}{p})} \mathbf{F}_{12}^{-\frac{q}{p}} |\mathbf{e}(t_r)|^{1-\frac{q}{p}}.$$

Proof: The reaching time is defined based on Lemma 2 and the value of settling time $t_{s,i}$ will define the terminal time T . At reaching time, $t_{r,i}$, the sliding surface is zero:

$$s_i(t_{r,i}) = \dot{e}_i + \beta \text{sign} \left(\sum_{j=1}^n K_{SP,ij}(\mathbf{x}) e_j \right) \left| \sum_{j=1}^n K_{SP,ij}(\mathbf{x}) e_j \right|^{\frac{q}{p}} = 0. \quad (23)$$

We consider the matrix-vector form of (23) for the sake of simplicity and rewrite it as:

$$\frac{d\mathbf{e}}{dt} = -\beta \mathbf{K}_{SP}(\mathbf{x}) \mathbf{e} |\mathbf{K}_{SP}(\mathbf{x}) \mathbf{e}|^{\frac{q}{p}-1}. \quad (24)$$

The upper bound of $\mathbf{K}_{SP}(\mathbf{x})$ will be considered to compute the integral

$$\frac{d\mathbf{e}}{dt} = -\beta \mathbf{K}_C \mathbf{e} |\mathbf{K}_C \mathbf{e}|^{\frac{q}{p}-1}, \quad (25)$$

where $\mathbf{K}_C = \mathbf{F}_{12}$ is the constant upper bound of $\text{eig}[\mathbf{K}_{SP}(\mathbf{x})] \leq \mathbf{K}_C$, stated in Assumption 1. Considering $\mathbf{K}_{SP}(\mathbf{x})$, the integration of Eq. (24) is not possible since the gain is a time-varying state-dependent value (related to error variable). We consider a constant gain \mathbf{K}_C for integration, then (25) is integrated as

$$-\frac{1}{\beta} \int_{\mathbf{e}(t_r)}^0 \frac{d\mathbf{e}}{(\mathbf{K}_C \mathbf{e}) |\mathbf{K}_C \mathbf{e}|^{\frac{q}{p}-1}} = -\frac{1}{\beta} \int_{\mathbf{e}(t_r)}^0 \frac{d\mathbf{e}}{(\mathbf{K}_C \mathbf{e}) (\sqrt{(\mathbf{K}_C \mathbf{e})^2})^{\frac{q}{p}-1}} = \int_{t_r}^{t_s+t_r} dt,$$

which results in

$$\begin{bmatrix} t_{s,1} \\ \vdots \\ t_{s,n} \end{bmatrix} \leq \frac{1}{\beta \left(1 - \frac{q}{p}\right)} \mathbf{K}_C^{-1} |\mathbf{K}_C \mathbf{e}(t_r)|^{1 - \frac{q}{p}}. \quad (26)$$

Considering Eq. (26) and if time tends to the final time of control task, t_f , the control gain goes to final boundary value, $\lim_{t \rightarrow t_f} \mathbf{K}_{SP}(\mathbf{x}(t)) = \mathbf{F}_{12}$. Each rows of right hand side of (26) define a settling time, $t_{s,i}$, for i -th error variable $e(t_{r,i})$. \mathbf{F}_{12} is a diagonal matrix with relatively large components, and it provides a situation where the i -th component dominates the rest of the arrays of $\mathbf{K}_{SP}(\mathbf{x}(t))$ in each row of the matrix. The nature of the finite-time gain of the SDDRE includes three phases: transient, steady-state, and final oscillations (due to the final weighting condition \mathbf{F}_{12}), Fig. 2.

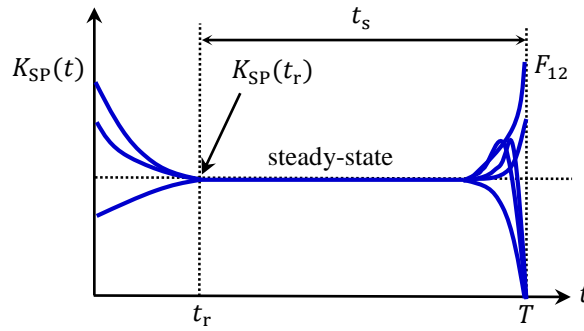


Fig. 2. The behavior of the SDDRE control gain.

Considering Fig. 2, the transient response is passed after reaching time, and after the steady-state value of the gain, the solution goes to the final boundary value. Finally, Eq. (26) is rewritten as

$$\begin{bmatrix} t_{s,1} \\ \vdots \\ t_{s,n} \end{bmatrix} \leq \frac{1}{\beta \left(1 - \frac{q}{p}\right)} \mathbf{F}_{12}^{-\frac{q}{p}} |\mathbf{e}(t_r)|^{1 - \frac{q}{p}}, \quad (27)$$

which defines the terminal time $T = \max(t_{r,i} + t_{s,i})$, and that concludes the proof. It perfectly makes sense; if one increases \mathbf{F}_{12} , it will force the system to a faster response, see Eq. (27), and results in a shorter $t_{s,i}$. ■

Remark 6. Theorem 2 expresses that the error of the system will converge to zero in finite time T , and this value is the shortest possible time, best case scenario.

Considering $\begin{bmatrix} t_{s,1} \\ \vdots \\ t_{s,n} \end{bmatrix} \leq \frac{1}{\beta(1-\frac{q}{p})} \mathbf{K}_{SP}^{-\frac{q}{p}}(t_{r,i}) |\mathbf{e}(t_r)|^{1-\frac{q}{p}}$ computes a more realistic

value, longer though finite, for the final time of error convergence.

Remark 7. The role of control over final time is played by the SDDRE control gain $\mathbf{K}_{SP}(\mathbf{x})$ in Eq. (6), tuned by weighting matrices $\mathbf{Q}(\mathbf{x})$, $\mathbf{R}(\mathbf{x})$ and \mathbf{F} .

Remark 8. The role of the chattering and elimination of that will be discussed in the simulation section. To keep the derivation intact based on the $\text{sign}(\cdot)$ function, saturation function was not considered in the derivation. However, to remove the chattering, saturation function or other similar ones such as $\tanh\left(\frac{\cdot}{\varepsilon}\right)$ could be used instead of $\text{sign}(\cdot)$ in implementation.

3. Dynamic Modeling of Flapping-wing Flying Robot

The weight of the body is light and the contribution of the aerodynamics of the wing is significant to the model. In reality, birds can perform various stable maneuvers during flight such as hovering, backward flight, diving, surging, etc. Such complete control over the motion expresses hybrid complex dynamics and continuous non-affine actuators. The mechanical design of a bird with all those properties might not be possible at the moment. This section intends to present a *simplified six-DoF model* of an FWFR with a *minimum* requirement of fully actuation mode. The coordinates and schematic model of the flapping-wing robot are presented in Fig. 3. The FWFR is not limited to a fully bioinspired design; so, a rudder was set on the tail for better control over the roll and yaw.

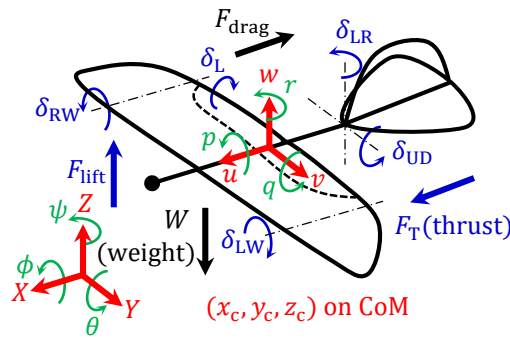


Fig. 3. The reference frame and model of the FWFR.

To cover a fully actuated model, six inputs are necessary, defined in Fig. 3. Why six inputs? There are several flapping robots controlled experimentally by only two inputs on their tail and one input thrust (generated by constant flapping) [37, 38, 40]. These models presented under-actuated systems subjected to many limitations with a lack of control over the motion. The landing was also like a fall by reducing the flapping frequency. Considering six actuators simplifies the control problem and extends the model to be used by so many methods, and closes the gap between the mechanical models and real birds. The three additional inputs are folding parts near the tip of the wings represented by δ_{RW} and δ_{LW} for the right and left wing; and a unified rudder on the back of the wings to enhance the lift. Observing the flapping birds, it can be realized that they are moving continuously possessing curved shapes and different parts for changing the lift force on the wing. So, the selected inputs are $\mathbf{u}(t) = [\delta_{RW}, \delta_{LW}, \delta_L, F_T, \delta_{UD}, \delta_{LR}]^T$ where $\delta_{(c)}$ (rad) represents the rudders and folding blades on the tails and wings and F_T (N) is thrust force caused by flapping of the wings.

The following assumptions are held for the modeling and behavior of the system:

1. The FWFR moves only forward in x_c axis direction. It can turn in a wide circular path; however, it cannot perform the lateral pure translation in y_c .
2. There is always a positive initial velocity condition for $u(0) = u_0$ where $u_0 > 0$. This represents throwing the FWFR to gain an initial lift and thrust for flight.
3. The flight path ought to be long enough for the FWFR to pass transient flight conditions. Specifically, $x_c(t_f)$ should be significantly greater than $y_c(t_f)$ and $z_c(t_f)$.
4. The FWFR motion avoids severe changes in orientation and the main changes are limited to small deviations due to the flapping.

The fixed reference frame is set by (X, Y, Z) , known as Earth frame; and the body (moving) coordinate is also presented by (x_c, y_c, z_c) placed on the center-of-mass (CoM) of the system. Four main forces are acting on the robot, the total weight of the system W , lift, drag, and thrust force. The generalized coordinates of the system are translation and orientation of the system in six-DoF, presented by $\mathbf{q}(t) = \{\xi_1(t), \xi_2(t)\}$ where $\xi_1(t) = [x_c(t), y_c(t), z_c(t)]^T$ (m) and $\xi_2(t) = [\phi(t), \theta(t), \psi(t)]^T$ (rad). On the body frame, local linear and angular velocities are named as $\{\mathbf{v}_1(t), \mathbf{v}_2(t)\}$ where $\mathbf{v}_1(t) =$

$[u(t), v(t), w(t)]^T$ (m/s) and $\mathbf{v}_2(t) = [p(t), q(t), r(t)]^T$ (rad/s). The kinematics relation between the global and local frame, considering *Flight-Assumption 4*, is presented [50]:

$$\dot{\xi}_1 = \mathbf{R}_{ZYX}(\xi_2)\mathbf{v}_1, \quad (28)$$

$$\dot{\xi}_2 = \mathbf{T}(\xi_2)\mathbf{v}_2, \quad (29)$$

where

$$\mathbf{R}_{ZYX}(\xi_2) = \begin{bmatrix} c_\theta c_\psi & s_\phi s_\theta c_\psi - c_\phi s_\psi & s_\phi s_\psi + c_\phi s_\theta c_\psi \\ c_\theta s_\psi & s_\phi s_\theta s_\psi + c_\phi c_\psi & -s_\phi c_\psi + c_\phi s_\theta s_\psi \\ -s_\theta & s_\phi c_\theta & c_\phi c_\theta \end{bmatrix},$$

$$\mathbf{T}(\xi_2) = \begin{bmatrix} 1 & s_\phi t_\theta & c_\phi t_\theta \\ 0 & c_\phi & -s_\phi \\ 0 & s_\phi/c_\theta & c_\phi/c_\theta \end{bmatrix},$$

in which e.g. $c_\theta = \cos(\theta(t))$ and $t_\theta = \tan(\theta(t))$.

The matrix $\mathbf{T}(\xi_2) = \mathbf{W}^{-1}(\xi_2)$ holds in which

$$\mathbf{v}_2 = \left[\mathbf{I}_{3 \times 3} \begin{bmatrix} \dot{\phi} \\ 0 \\ 0 \end{bmatrix}; \mathbf{R}_X(\phi) \begin{bmatrix} 0 \\ \dot{\theta} \\ 0 \end{bmatrix}; \mathbf{R}_X(\phi)\mathbf{R}_Y(\theta) \begin{bmatrix} 0 \\ 0 \\ \dot{\psi} \end{bmatrix} \right] = \begin{bmatrix} 1 & 0 & -s_\theta \\ 0 & c_\phi & c_\theta s_\phi \\ 0 & -s_\phi & c_\theta c_\phi \end{bmatrix} \dot{\xi}_2 = \mathbf{W}(\xi_2)\dot{\xi}_2,$$

and $\mathbf{W}(\xi_2)$ is invertible if $\det(\mathbf{W}(\xi_2)) = \cos \theta \neq 0$. The kinematics, Eqs. (28) and (29), and the reference frames are in the common forms of flying objects in the aerospace community such as aircraft, quadcopters, etc. The dynamics of the FWFR is

$$\mathbf{M}(\mathbf{q})\ddot{\mathbf{q}} + \mathbf{C}(\mathbf{q}, \dot{\mathbf{q}})\dot{\mathbf{q}} + \mathbf{D}(\mathbf{q}, \dot{\mathbf{q}})\dot{\mathbf{q}} + \mathbf{g}(\mathbf{q}) = \mathbf{U}, \quad (30)$$

where $\mathbf{M}(\mathbf{q}): \mathbb{R}^6 \rightarrow \mathbb{R}^{6 \times 6}$ is the inertia matrix, $[\mathbf{C}(\mathbf{q}, \dot{\mathbf{q}})\dot{\mathbf{q}}]: \mathbb{R}^6 \times \mathbb{R}^6 \rightarrow \mathbb{R}^6$ is Coriolis and centrifugal forces, $[\mathbf{D}(\mathbf{q}, \dot{\mathbf{q}})\dot{\mathbf{q}}]: \mathbb{R}^6 \times \mathbb{R}^6 \rightarrow \mathbb{R}^6$ collects drag and aerodynamics terms, $\mathbf{g}(\mathbf{q}): \mathbb{R}^6 \rightarrow \mathbb{R}^6$ is gravity vector and $\mathbf{U} \in \mathbb{R}^6$ is input vector:

$$\mathbf{M}(\mathbf{q}) = \begin{bmatrix} m \times \mathbf{I}_{3 \times 3} & \mathbf{0}_{3 \times 3} \\ \mathbf{0}_{3 \times 3} & \mathbf{J}(\xi_2) \end{bmatrix}, \mathbf{C}(\mathbf{q}, \dot{\mathbf{q}}) = \begin{bmatrix} \mathbf{0}_{3 \times 3} & \mathbf{0}_{3 \times 3} \\ \mathbf{0}_{3 \times 3} & \bar{\mathbf{C}}(\xi_2, \dot{\xi}_2) \end{bmatrix}, \mathbf{D}(\mathbf{q}, \dot{\mathbf{q}}) = \begin{bmatrix} \bar{\mathbf{D}}(\dot{\xi}_2) & \mathbf{0}_{3 \times 3} \\ \mathbf{0}_{3 \times 3} & \mathbf{0}_{3 \times 3} \end{bmatrix}, \mathbf{g}(\mathbf{q}) = [0, 0, mg, 0, 0, 0]^T,$$

in which m (kg) is the total mass of the FWFR, $g \left(\frac{m}{s^2}\right)$ is gravity constant, and:

$$\mathbf{J}(\xi_2) = \mathbf{W}^T(\xi_2)\mathbf{I}\mathbf{W}(\xi_2),$$

$$\mathbf{I} = \text{diag}(I_{xx}, I_{yy}, I_{zz}),$$

$$\begin{aligned}
 \bar{C}_{11}(\xi_2, \xi_2) &= 0, \bar{C}_{12}(\xi_2, \xi_2) = \frac{(I_{yy} - I_{zz})(\dot{\theta}s_{2\phi} - \dot{\psi}c_{2\phi}c_{\theta})}{2}, \bar{C}_{13}(\xi_2, \xi_2) \\
 &= -\dot{\theta} \left(I_{xx}c_{\theta} + \frac{c_{\theta}(I_{yy} - I_{zz})c_{2\phi}}{2} \right) - (I_{yy} - I_{zz})\dot{\psi}c_{\phi}c_{\theta}^2s_{\phi}, \bar{C}_{21}(\xi_2, \xi_2) = \frac{I_{xx}\dot{\psi}c_{\theta}}{2}, \bar{C}_{22}(\xi_2, \xi_2) \\
 &= -\frac{(I_{yy} - I_{zz})s_{2\phi}(4\dot{\phi} - \dot{\psi}s_{\theta})}{4}, \bar{C}_{23}(\xi_2, \xi_2) \\
 &= \dot{\phi} \left(\frac{I_{xx}c_{\theta}}{2} + (I_{yy} - I_{zz})c_{2\phi}c_{\theta} \right) - \frac{(I_{yy} - I_{zz})\dot{\theta}s_{2\phi}s_{\theta}}{4} \\
 &+ \dot{\psi}c_{\theta}s_{\theta} \left(\frac{I_{yy}}{2} - I_{xx} + \frac{I_{zz}}{2} - \frac{I_{yy}c_{2\phi}}{2} + \frac{I_{zz}c_{2\phi}}{2} \right), \bar{C}_{31}(\xi_2, \xi_2) = -I_{xx}\dot{\theta}c_{\theta}, \bar{C}_{32}(\xi_2, \xi_2) \\
 &= \frac{(I_{yy} - I_{zz})(2\dot{\phi}c_{2\phi}c_{\theta} - \dot{\theta}s_{2\phi}s_{\theta})}{2}, \bar{C}_{33}(\xi_2, \xi_2) \\
 &= \dot{\phi}s_{2\phi}(I_{yy} - I_{zz}) \left(\frac{c_{2\theta}}{2} + \frac{1}{2} \right) - \dot{\theta}s_{2\theta} \left(\frac{I_{yy}}{2} - I_{xx} + \frac{I_{zz}}{2} - \frac{I_{yy}c_{2\phi}}{2} + \frac{I_{zz}c_{2\phi}}{2} \right).
 \end{aligned}$$

The drag matrix in the translation part is defined as $\bar{\mathbf{D}}(\xi_2) = \frac{\rho}{2} \text{diag}(A_x C_{Dx} \dot{x}_c, A_y C_{Dy} \dot{y}_c, A_z C_{Dz} \dot{z}_c)$ where A_i is the effective area of the system in i axis and C_{Di} is the drag constant for $i = x, y, z$. Based on Flight-Assumption 4, the drag and aerodynamics effect in orientation dynamics are neglected.

The input vector includes two force and torque parts:

$$\mathbf{U} = \begin{bmatrix} X, Y, Z, L, M, N \end{bmatrix}^T.$$

force
torque

The force/torque vector \mathbf{U} has a nonlinear complicated relation with ultimate input vector \mathbf{u} , which is nonlinear non-affine and unknown:

$$\mathbf{U} = \mathbf{F}(\mathbf{q}, \dot{\mathbf{q}}, \mathbf{u}). \quad (31)$$

Representation of the Eq. (31) using Taylor series expansion around zero is

$$\mathbf{U} = \mathbf{F}(\mathbf{q}, \dot{\mathbf{q}}, \mathbf{0}) + \frac{\partial \mathbf{F}(\mathbf{q}, \dot{\mathbf{q}}, \mathbf{0})}{\partial \mathbf{u}} \mathbf{u} + \frac{1}{2} \frac{\partial^2 \mathbf{F}(\mathbf{q}, \dot{\mathbf{q}}, \mathbf{0})}{\partial \mathbf{u}^2} \mathbf{u}^2 + \dots \quad (32)$$

All the rows of vector $\mathbf{F}(\mathbf{q}, \dot{\mathbf{q}}, \mathbf{u})$ are multiplied by \mathbf{u} , or in other words, $\mathbf{F}(\mathbf{q}, \dot{\mathbf{q}}, \mathbf{0}) = \mathbf{0}$. Considering the equilibrium $\mathbf{F}(\mathbf{q}, \dot{\mathbf{q}}, \mathbf{0}) = \mathbf{0}$ and neglecting the higher terms of the Taylor series, Eq. (32) is approximated by

$$\mathbf{U} = \frac{\partial \mathbf{F}(\mathbf{q}, \dot{\mathbf{q}}, \mathbf{0})}{\partial \mathbf{u}} \mathbf{u} = \begin{bmatrix} X_{\delta_{RW}} & X_{\delta_{LW}} & X_{\delta_L} & X_{F_T} & X_{\delta_{UD}} & X_{\delta_{LR}} \\ Y_{\delta_{RW}} & Y_{\delta_{LW}} & Y_{\delta_L} & Y_{F_T} & Y_{\delta_{UD}} & Y_{\delta_{LR}} \\ Z_{\delta_{RW}} & Z_{\delta_{LW}} & Z_{\delta_L} & Z_{F_T} & Z_{\delta_{UD}} & Z_{\delta_{LR}} \\ L_{\delta_{RW}} & L_{\delta_{LW}} & L_{\delta_L} & L_{F_T} & L_{\delta_{UD}} & L_{\delta_{LR}} \\ M_{\delta_{RW}} & M_{\delta_{LW}} & M_{\delta_L} & M_{F_T} & M_{\delta_{UD}} & M_{\delta_{LR}} \\ N_{\delta_{RW}} & N_{\delta_{LW}} & N_{\delta_L} & N_{F_T} & N_{\delta_{UD}} & N_{\delta_{LR}} \end{bmatrix} \begin{bmatrix} \delta_{RW} \\ \delta_{LW} \\ \delta_L \\ F_T \\ \delta_{UD} \\ \delta_{LR} \end{bmatrix}, \quad (33)$$

where i.e. $X_{\delta_{RW}} = \frac{\partial X}{\partial \delta_{RW}}$. We call the coefficient matrix $\mathbf{M}_x = \frac{\partial \mathbf{F}(\mathbf{q}, \dot{\mathbf{q}}, \mathbf{0})}{\partial \mathbf{u}}$ a mixer matrix. In reality, for example, considering a real bird, it could be expected that all the inputs \mathbf{u} contribute to the force/torque vector \mathbf{U} and all the elements of the mixer have values; however, this model is simplified by several assumptions. To find the effective elements of the mixer, the effect of the inputs are considered in decoupled mode, then based on Fig. 3, one could rewrite Eq. (33) as:

$$\mathbf{U} = \begin{bmatrix} X_{\delta_{RW}} & -X_{\delta_{LW}} & 0 & X_{F_T} \cos \psi & 0 & X_{\delta_{LR}} \\ -Y_{\delta_{RW}} & Y_{\delta_{LW}} & 0 & Y_{F_T} \sin \psi & 0 & Y_{\delta_{LR}} \\ 0 & 0 & Z_{\delta_L} & Z_{F_T} \cos \theta & Z_{\delta_{UD}} & 0 \\ L_{\delta_{RW}} & L_{\delta_{LW}} & 0 & 0 & 0 & 0 \\ 0 & 0 & M_{\delta_L} & 0 & M_{\delta_{UD}} & 0 \\ 0 & 0 & 0 & 0 & 0 & N_{\delta_{LR}} \end{bmatrix} \begin{bmatrix} \delta_{RW} \\ \delta_{LW} \\ \delta_L \\ F_T \\ \delta_{UD} \\ \delta_{LR} \end{bmatrix}.$$

The oscillation effect of flapping is more visible in z_c axis and pitch angle θ . Based on the flapping oscillation, a disturbance vector is applied to the dynamics, added to the system in state-space representation. The inputs are also bounded between $\delta_{\min} \leq \delta_{(\cdot)} \leq \delta_{\max}$ and $0 \leq F_T \leq F_{T,\max}$.

4. State-space Form and Implementation

The state variable of the system is selected as

$$\mathbf{x} = [\xi_1^T, \xi_2^T, \mathbf{v}_1^T, \mathbf{v}_2^T]^T = [x_c, y_c, z_c, \phi, \theta, \psi, u, v, w, p, q, r]^T. \quad (34)$$

Considering the state vector (34) and the dynamics (30), the state-space form is obtained

$$\dot{\mathbf{x}} = \begin{bmatrix} \mathbf{R}_{ZYX}(\xi_2)\mathbf{v}_1 \\ \mathbf{T}(\xi_2)\mathbf{v}_2 \\ \mathbf{M}^{-1}(\mathbf{q})(\mathbf{U} - \mathbf{C}(\mathbf{q}, \dot{\mathbf{q}})\dot{\mathbf{q}} - \mathbf{D}(\mathbf{q}, \dot{\mathbf{q}})\dot{\mathbf{q}} - \mathbf{g}(\mathbf{q}) - \mathbf{D}_F) \end{bmatrix}, \quad (35)$$

where $\mathbf{D}_F = d_F \times [0, 0, \cos \omega t, 0, 0, 0]^T$ is the disturbance caused by flapping in which d_F is the amplitude of the oscillatory disturbance.

Comparing Eq. (35) with (2), the values of $\mathbf{f}(\mathbf{q}, \dot{\mathbf{q}}) = -\mathbf{M}^{-1}(\mathbf{q})(\mathbf{C}(\mathbf{q}, \dot{\mathbf{q}})\dot{\mathbf{q}} + \mathbf{D}(\mathbf{q}, \dot{\mathbf{q}})\dot{\mathbf{q}} + \mathbf{g}(\mathbf{q}))$ and $\mathbf{E}(\mathbf{q}) = \mathbf{M}^{-1}(\mathbf{q})$ are defined. The SDC parameterization matrices are also shaped as

$$\begin{aligned} \mathbf{A}_t(\mathbf{x}) &= \begin{bmatrix} \mathbf{0}_{3 \times 3} & | & \mathbf{R}_{ZYX}(\xi_2) \\ \hline \mathbf{0}_{3 \times 3} & | & -1/m\bar{\mathbf{D}}(\xi_2) \end{bmatrix}, \mathbf{A}_o(\mathbf{x}) \\ &= \begin{bmatrix} \mathbf{0}_{3 \times 3} & | & \mathbf{T}(\xi_2) \\ \hline \mathbf{0}_{3 \times 3} & | & -\mathbf{J}^{-1}(\xi_2)\mathbf{C}(\mathbf{q}, \dot{\mathbf{q}}) \end{bmatrix}, \mathbf{B}_t(\mathbf{x}) = \begin{bmatrix} \mathbf{0}_{3 \times 3} \\ \hline \frac{1}{m}\mathbf{I}_{3 \times 3} \end{bmatrix}, \mathbf{B}_o(\mathbf{x}) = \begin{bmatrix} \mathbf{0}_{3 \times 3} \\ \hline \mathbf{J}^{-1}(\xi_2) \end{bmatrix}, \end{aligned}$$

which results in the gain $\mathbf{K}_{SP}(\mathbf{x}) = \text{diag}(\mathbf{K}_{SP_t}(\mathbf{x}), \mathbf{K}_{SP_o}(\mathbf{x}))$. The nature of the orientation dynamic is faster than the translation. To solve the Riccati easier and avoid setting the eigenvalues of the dynamics near the imaginary axis, two separate SDDRE control is used.

It should be noted that considering the smooth and small variation of orientation variables, $\mathbf{R}_{ZYX}(\xi_2)$ and $\mathbf{T}(\xi_2)$ possess almost identity matrices. That is necessary to guarantee the controllability and observability conditions, Condition 1 and 2. The rest of the design is based on Section 2-3.

5. Simulations

5-1. Illustrative Example

A Van der Pole oscillator is simulated and compared with two other controllers. The state-space representation of the disturbed Van der Pole equation is [12]:

$$\dot{\mathbf{x}} = \begin{bmatrix} 0 & 1 \\ -1 & 1 - x_1^2 \end{bmatrix} \mathbf{x} + \begin{bmatrix} 0 \\ 1 \end{bmatrix} u + \begin{bmatrix} 0 \\ \text{rand}(1) \times 0.2 \sin 100t \end{bmatrix},$$

where $\Psi(t) = \text{rand}(1) \times 0.2 \sin 100t$ is an external disturbance in which $\text{rand}(1)$ generates a random number between 0 and 1 at each time-step of the simulation. The proposed method is finite-time and robust. It is good to compare with the SDDRE controller which is finite time though is not robust and also with the conventional TSMC which lacks optimality. The initial condition is $\mathbf{x}(0) = [2, 1]^T$ and the system is to be regulated to the equilibrium point. The control parameters are selected as $R = 1$, $\mathbf{Q} = \mathbf{I}_{2 \times 2}$, $\mathbf{F} = 10 \times \mathbf{Q}$, $\eta = 2$, $\beta = 1.5$, $q = 7$, and $p = 9$.

We also consider $\hat{f}(\mathbf{x}) = 1.2 \times (-x_1 + (1 - x_1^2)x_2)$, $\hat{E} = 1.1$, and $\Psi_c(t) = 0.2 \sin 100t$ which defines (for example here we considered $\text{rand}(1) = 0.501$) the constants, based on Eqs. (10)-(12):

$$\Psi_0 = |\max(\Psi) - E\hat{E}^{-1} \max(\Psi_c)| = |0.1060 - E\hat{E}^{-1}0.2| = 0.0758,$$

$$f_0 = |f(\mathbf{x}) - E\hat{E}^{-1}\hat{f}(\mathbf{x})| = \left| \left(\frac{1}{1.2} - E\hat{E}^{-1} \right) \hat{f}(\mathbf{x}) \right| = 0.0758|\hat{f}(\mathbf{x})|,$$

$$E_{\max} = E_{\min} = E\hat{E}^{-1} = 0.9091.$$

The parameters of the SDDRE and TSMC controllers are similar weighting matrices and parameters. The only change in the TSMC is the constant gain of $K_{SP} = 1$. The comparisons have been done in different terminal times to illustrate the role of predefined time-setting in the results. The error and input of the system in different final times are presented in Fig. 4 and the error details are in Table 1. The error of the proposed TSMC was obtained less than the TSMC and SDDRE which showed for a system with uncertainty, a combination of the robust and optimal control could score better results. For the 6s final time, the proposed TSMC improved¹ w.r.t. the TSMC 61% and SDDRE 61.3%; for the 4s final time, the proposed TSMC improved w.r.t. the TSMC 56.3% and SDDRE 87.3%; and for the 2s final time, the proposed TSMC improved w.r.t. the TSMC 82.4% and SDDRE 47.2%. Based on the presented data in Ref. [12], for $t_f = 4s$, the proposed TSMC response has been validated. Setting the final time as an input with two sliding surfaces was proposed in Ref. [12], though in this current work, a unified sliding surface is considered with additional sub-optimality in the gain.

Table 1. The error details of the Van der Pole system in different final times.

error at	$t_f = 6s$	$t_f = 4s$	$t_f = 2s$
TSMC	0.0138	0.0138	1.1773
SDDRE	0.0139	0.0478	0.3914
Proposed TSMC	0.0054	0.0060	0.2063

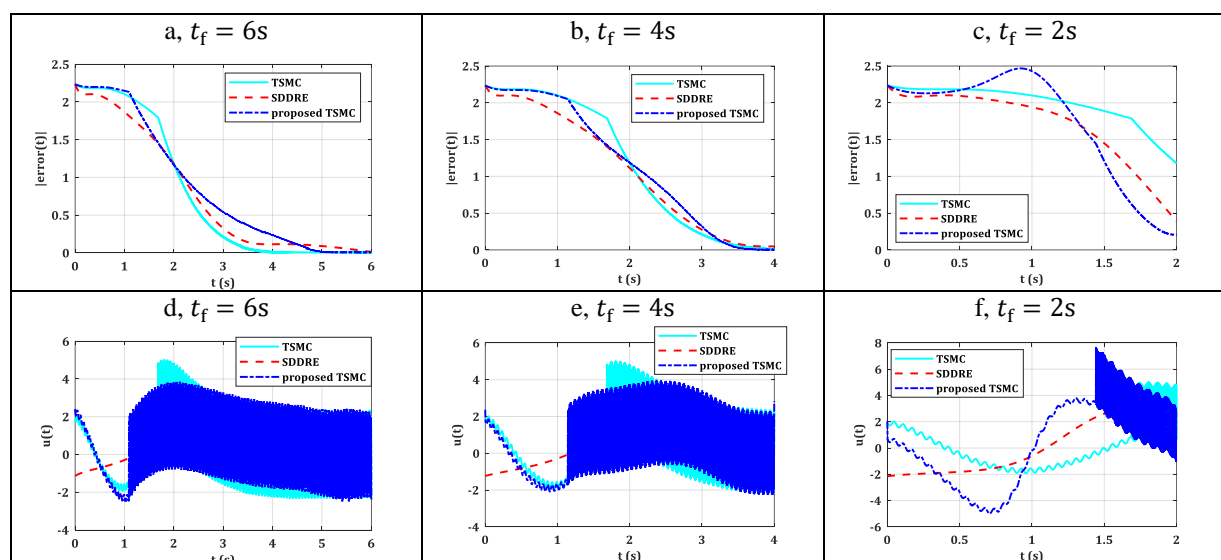


Fig. 4. The error and input of the system in different final times, Van der Pole oscillator.

¹ Possible improvement (%): $\frac{\text{old data} - \text{new data}}{\text{old data}} \times 100$

The chattering effect on the input is always an issue in the implementation of the different kinds of sliding mode controllers. Here we also observe the chattering in the input signals, Fig. 4 (d)-(f). For the sake of simplicity and derivations in the proof, it is better to consider the sign function in the process. Also, the sign function acts more precisely in finite-time regulation. For practical implementation and having an input signal without chattering, a saturation function or other similar ones such as $\tanh\left(\frac{\cdot}{\varepsilon}\right)$ could be used. Here we considered $\tanh\left(\frac{\cdot}{\varepsilon}\right)$ where $\varepsilon = 0.1$. The simulated Van der Pole with saturation function has resulted in Fig. 5. The error of the TSMC was gained 1.1817, SDDRE 0.3914, and proposed TSMC 0.2051 which outranked the other two. So, chattering is not a problem throughout this research and common functions for removing that show good performance as well.

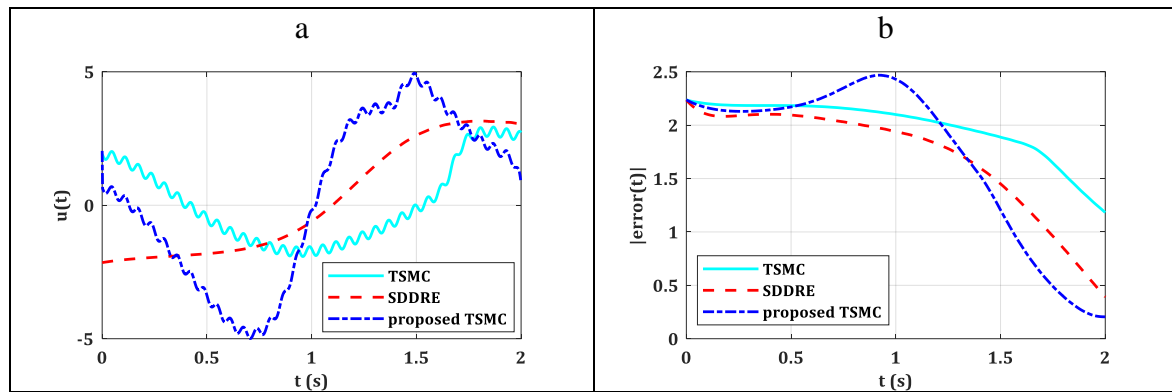


Fig. 5. Input signal and error of the Van der Pole using saturation function, chattering-free mode.

Time analysis: Considering the final time of control problem $t_f = 6s$, the reaching time for conventional TSMC is found $t_r = 1.78s$, settling time $t_s = 2.89s$ and the terminal time $T = 4.67s$. The states, error, and sliding surface are illustrated in Fig. 6-a. The phase plane of the systems is shown in Fig. 6-b. The error at the terminal time was gained $e(T = 4.67) = 0.0076$ and at $e(t_f = 6) = 0.0138$, both of them in the steady-state range of error bound 0.02. Simulation of the proposed TSMC (with SDRE gain $K_{SP}(\mathbf{x})$) resulted in shorter reaching time $t_r = 1.15s$, longer settling time $t_s = 6.67s$ and terminal time $T = 7.83s$. However, error at final time was found $e(t_f = 6) = 0.0054$, with 28.9% more precision. It should be noted that with this proposed design, the value of the error at the final time t_f is important, not the settling time. Reducing the final time, results in $e(t_f = 5) = 0.0067$, and $e(t_f = 4) = 0.0060$, both of them less than $e(T = 4.67)$ of conventional TSMC.

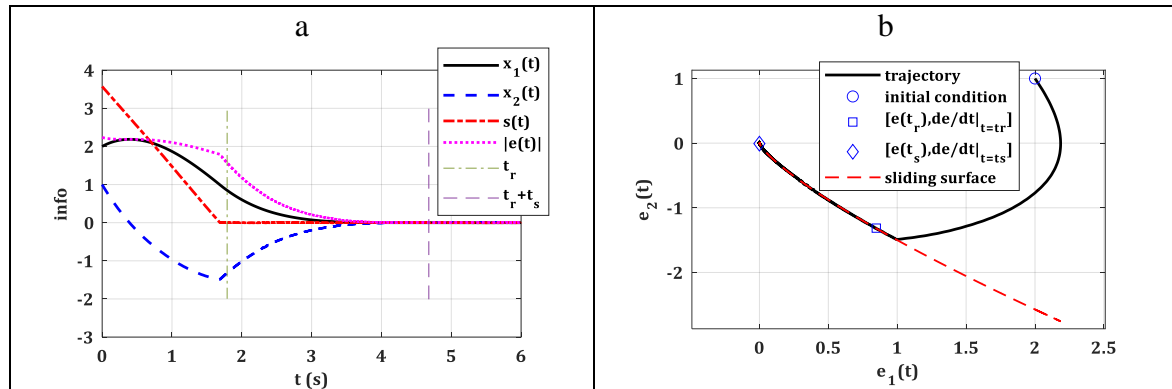


Fig. 6. (a) the state information; (b) phase plane.

5-2. Flapping-Wing Flying Robot

The characteristics of the robot define the behavior of the system; the weight of an FWFR prototype is usually less than 1 (kg). The aerodynamics force and drag in the FWFR case play an important role. Unlike aircraft, during the regulation in X axis, there are significant variations in other directions as well and therefore, aerodynamics force and drag should be included in three axes. The tuning of the controller is sensitive and dependent on the initial and final conditions. The physical characteristics of a sample FWFR are reported in Table 2.

Table 2. Parameters and specifications of the FWFR.

parameter	value	unit	description
I_{xx}	0.0026	kgm ²	moment of inertia around X axis
I_{yy}	0.0010	kgm ²	moment of inertia around Y axis
I_{zz}	0.0071	kgm ²	moment of inertia around Z axis
m	0.535	kg	total mass of the system
g	9.81	m/s ²	gravity constant
ρ	1.225	kg/m ³	air density
A_x	0.15	m ²	effective area of system in X axis
A_y	0.24	m ²	effective area of system in Y axis
A_z	0.4	m ²	effective area of system in Z axis
$C_{D,x}, C_{D,y}, C_{D,z}$	0.045	—	drag coefficient in X, Y, Z axes

The actuator limitations are applied by $-\frac{\pi}{6} \leq \delta_{(\cdot)} \leq \frac{\pi}{6}$ and $-0.5248 \leq F_T \leq 7.8725$. The elements of the mixer matrix are also considered as:

$$\begin{aligned}
 X_{\delta_{RW}} &= 0.05, X_{\delta_{LW}} = -X_{\delta_{RW}}, X_{F_T} = 1.5, X_{\delta_{LR}} = 2.45, \\
 Y_{\delta_{LR}} &= X_{\delta_{LR}}, Y_{F_T} = X_{F_T}, Y_{\delta_{RW}} = 0.75, Y_{\delta_{LW}} = Y_{\delta_{RW}}, \\
 Z_{\delta_L} &= 50.3, Z_{F_T} = 1.57, Z_{\delta_{UD}} = 1.75, L_{\delta_{RW}} = 0.67, \\
 L_{\delta_{LW}} &= L_{\delta_{RW}}, M_{\delta_L} = 1.74, M_{\delta_{UD}} = 1.4, N_{\delta_{LR}} = 0.00224.
 \end{aligned}$$

Then the inputs could be found by $\mathbf{u} = \mathbf{M}_x^{-1}\mathbf{U}$, where the limits are applied by

$$u_i = \begin{cases} u_i \geq u_{\max}, & u_i = u_{\max}, \\ u_i, & u_{\min} < u_i < u_{\max}, \\ u_i \leq u_{\min}, & u_i = u_{\min}. \end{cases}$$

The main effects of disturbance caused by flapping are in z_c , hence the disturbance vector is considered in the system (35) to complete the modeling, in which $\omega = 30 \left(\frac{\text{rad}}{\text{s}}\right)$ is flapping frequency and $d_F = 0.1$. Based on the assumption of the modeling the trajectory should be long enough in X axis direction. The initial condition is regarded as zero except the initial velocity of $u(0) = 1 \left(\frac{\text{m}}{\text{s}}\right)$ and angle $\theta(0) = -\frac{\pi}{12}$ (rad), which means throwing the FWFR to the air, $\mathbf{x}(0) = [0,0,0,0, -\pi/12,0,1,0,0,0,0,0]^T$. The final condition is $\mathbf{x}(t_f) = [15, -5,2,0.344, -0.132, -0.321, \mathbf{0}_{1 \times 6}]^T$ and the simulation time is chosen 15 (s).

The control gain selection is quite sensitive due to the flight conditions and limitations of the model. The tuning process includes SDRE and TSMC gain selection. The first step is to define the weighting matrices of the SDRE without considering the TSMC, then with stable SDRE tuning, the TSMC must be added to the control law. The SDRE matrices are as follow $\mathbf{R}_t = \mathbf{R}_o = \mathbf{I}_{3 \times 3}$, $\mathbf{Q}_t = \text{diag}(\mathbf{0.25}_{1 \times 3}, \mathbf{1.75}_{1 \times 3})$, $\mathbf{Q}_o = \text{diag}(\mathbf{0.00002}_{1 \times 3}, \mathbf{0.0001}_{1 \times 3})$, $\mathbf{F}_t = 100\mathbf{Q}_t$ and $\mathbf{F}_o = 5\mathbf{Q}_o$ where $\mathbf{0.1}_{1 \times 3} = [0.1,0.1,0.1]$ where i.e. $\mathbf{0.25}_{1 \times 3} = [0.25,0.25,0.25]$. The terminal sliding mode will add robustness to the SDRE terminal-time gain. Tuning the TSMC also presents $\boldsymbol{\eta} = [1,1,1,0.1,0.1,0.05]^T$, $\beta = 1$, $q = 7$, and $p = 9$ (q and p are the power of absolute terms in Eq. (8)). For the combination of the TSMC plus SDDRE, the orientation weighting matrices must be changed to $\mathbf{Q}_o = \mathbf{I}_{6 \times 6}$. Simulating the model, the position variables are presented in Fig. 7. The orientation variables of the system are depicted in Fig. 8. The desired orientation angles were defined based on the geometry of the initial and final position to keep the system aligned in a straight line that connects both points. The linear and angular velocities of the FWFR are presented in Fig. 9 and Fig. 10. The control input force and moments are presented in Fig. 11. The nature of the TSMC imposes chattering on the control signals that could be amended by the use of saturation function; however, this reduces the precision in finite-time control. The trajectory of the system is shown in Fig. 12. The rudder angles of the left and right wings are shown in Fig. 13 a-b with respect. The variation of the lifting rudder on the rear edge of the wing is illustrated in Fig. 13 c. The necessary generated thrust by flapping is shown in Fig. 13 d. And finally, the angles of upper/down and left/right rudders on the tail are presented in Fig. 13 e-f. The error was found 0.4395mm. The chattering

removal of the inputs Fig. 13, by using tanh function and $\varepsilon = 0.1$ present practical inputs for rudders and thrusts Fig. 14; with the expense of more error in regulation 1.8781mm.

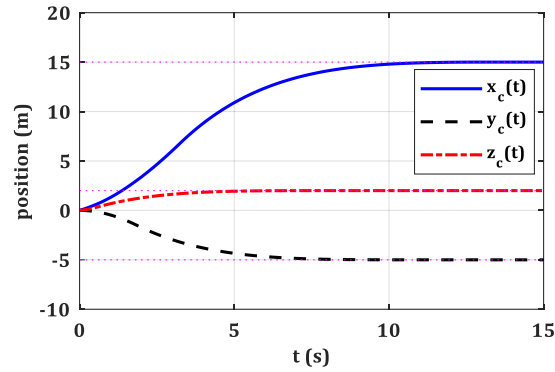


Fig. 7. The position variable of the FWFR.

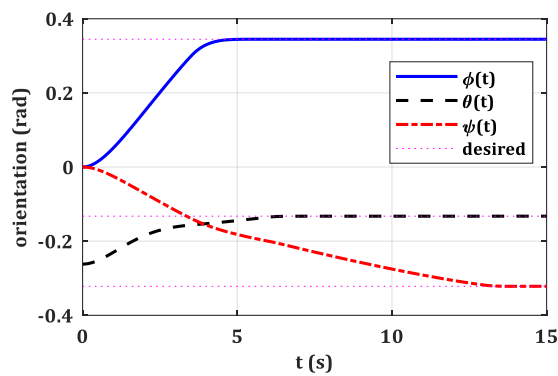


Fig. 8. The orientation of the system in regulation.

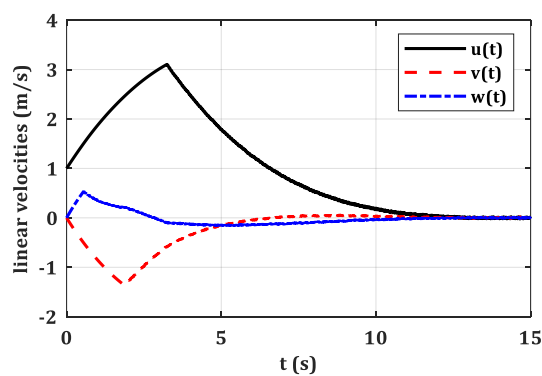


Fig. 9. Linear velocities of the FWFR in local coordinates.

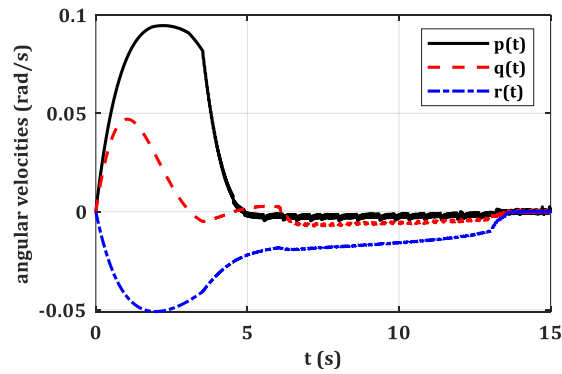


Fig. 10. Angular velocities of the system.

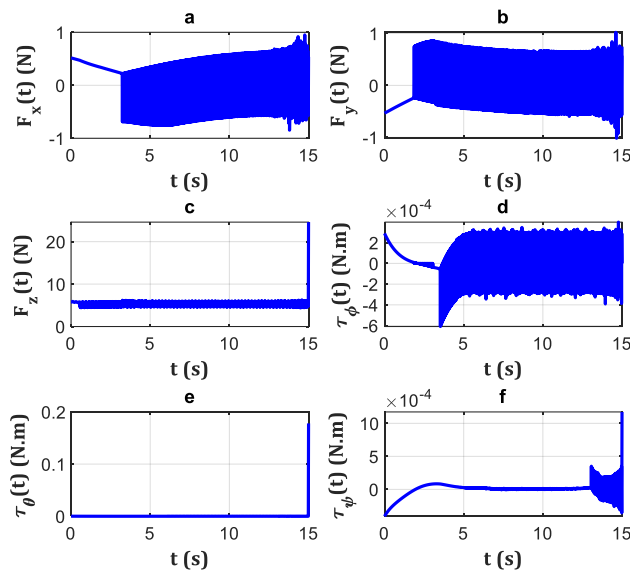


Fig. 11. (a)-(c)The control input force; (d)-(f) and moments.

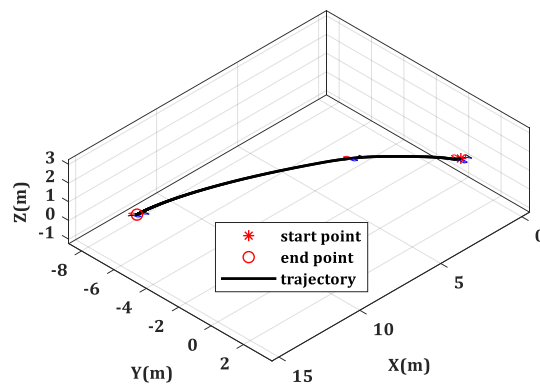


Fig. 12. The trajectory of the system in regulation.

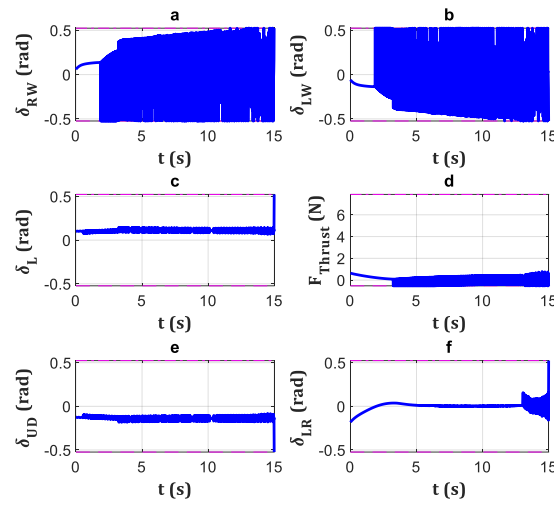


Fig. 13. (a) The rudder angle at the tip of the right-wing; (b) the rudder angle at the tip of the left-wing; (c) the lift rudder angle at the rear edge of the wing; (d) generated thrust by flapping; (e) the upper/down rudder angel at the tail; (f) the left/right rudder angel at the tail.

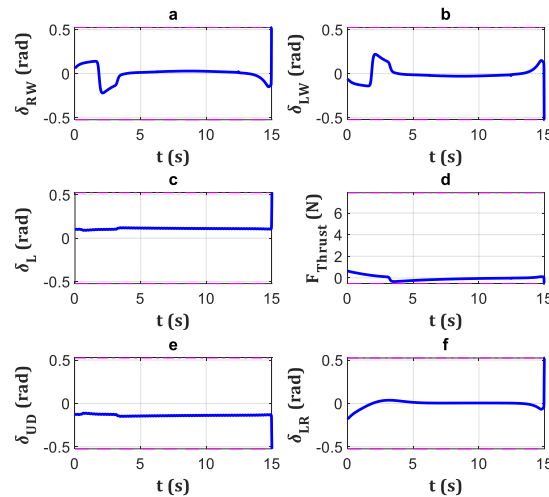


Fig. 14. Chattering removal approach. (a) The rudder angle at the tip of the right-wing; (b) the rudder angle at the tip of the left-wing; (c) the lifting rudder angle at the rear edge of the wing; (d) generated thrust by flapping; (e) the upper/down rudder angel at the tail; (f) the left/right rudder angel at the tail (chattering removal results).

5-3. Comparison and Validation of FWFR results

To check the performance of the proposed controller applied to complex systems, the flight simulation has been validated with other controllers as well. Similar to Section 5-1, SDDRE represents an optimal finite-time controller and the conventional TSMC represents a robust one. The PD+gravity has been also selected to check the system with a simple structured

controller, too. The gains of the controllers are similar to Section 5-2 for TSMC and proposed TSMC. The PD+gravity controller gains are $\mathbf{K}_{P,t} = 0.5 \times \mathbf{I}_{3 \times 3}$ and $\mathbf{K}_{D,t} = 1.5 \times \mathbf{I}_{3 \times 3}$ for translation control; and $\mathbf{K}_{P,o} = 0.005 \times \mathbf{I}_{3 \times 3}$ and $\mathbf{K}_{D,o} = 0.01 \times \mathbf{I}_{3 \times 3}$ for the orientation part. The gains of the SDDRE were also set similar to Section 5-2. Conducting the simulation with the same conditions in Section 5-2, the results are presented in Fig. 15. The error of the regulation by the mentioned controllers is presented in Fig. 15. The details of the errors are reported in Table 3. The proposed method gained the least error 0.43mm using sign function. The chattering-free version of the controller also gained 1.87mm error which is acceptable concerning 15m regulation distance. Since the time of regulation was long enough for all the controllers, the difference between the proposed TSMC 0.43mm and conventional TSMC 0.53mm is negligible. However, decreasing the final time will show better results for the proposed TSMC similar to Section 5-1.

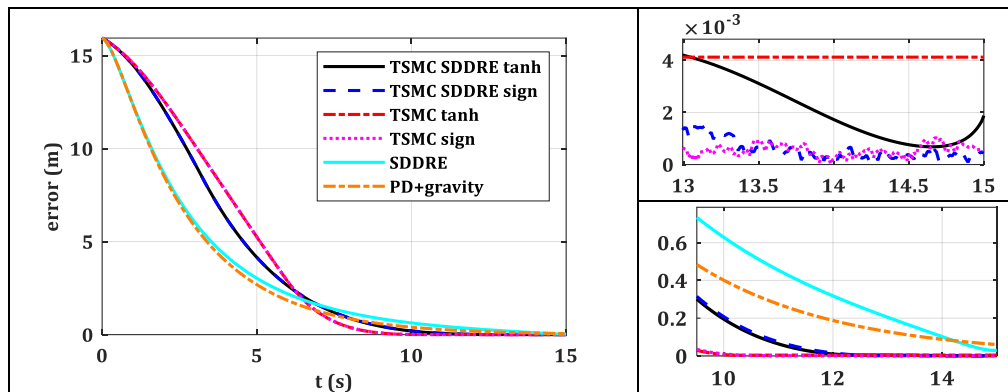


Fig. 15. The error of the FWFR, controlled by proposed TSMC, PD+gravity, TSMC, and SDDRE.

Table 3. The details of the error with different control methods.

method	error (mm)
TSMC, SDDRE, tanh	1.8781
TSMC, SDDRE, sign	0.4395
TSMC, tanh	4.1253
TSMC, sign	0.5380
SDDRE	29.2899
PD+gravity	60.0328

6. Conclusions

A novel terminal sliding mode control approach using the state-dependent differential Riccati equation is introduced. Finite-time control has been always a good option in control engineering. The conventional TSMC is a continuous finite-time controller; however, the desired final time is not commanded directly. The SDDRE presents a finite control gain that

penalizes the states near the final time. Instead of using the standard SDDRE control law, the gain is extracted and partitioned to be used in the definition of the sliding surface. The new nonlinear sliding surface presented a novel TSMC with the possibility of finite-time control as an input parameter. The Lyapunov stability criteria were used to deliver a stable adaptive gain to the TSMC. The proposed controller was validated by simulation of a Van der Pole oscillator [12]. The results were similar to the available data and also proposed TSMC scored 61% improvement in comparison with conventional TSMC and 61.3% with SDDRE; for the 6s final time. To check the performance of the controller, a complex model was also simulated. The flapping wing flying robot possesses nonlinear uncertain dynamics which is a challenging case in the control field. The proposed TSMC controlled the model successfully and was compared with SDDRE and conventional TSMC to validate the results. The superiority of the proposed TSMC was also shown by 18.3% improvement concerning conventional TSMC, 93.5% over SDDRE, and 96.8% over PD+gravity.

Acknowledgments

This work is supported by the European Research Council as part of GRIFFIN ERC advanced Grant 2017, Action 788247; and by the European Commission H2020 Programme AERIAL-CORE, contract number 871479.

Supplementary material: The MATLAB codes of the simulation section have been provided as supplementary material of the paper.

Appendix 1: Derivative of the sliding surface.

The sliding surface is rewritten as

$$s_i = \dot{e}_i + \beta \frac{\sum_{j=1}^n K_{SP,ij}(\mathbf{x})e_j}{\left|\sum_{j=1}^n K_{SP,ij}(\mathbf{x})e_j\right|} \left|\sum_{j=1}^n K_{SP,ij}(\mathbf{x})e_j\right|^{\frac{q}{p}}$$

$$= \dot{e}_i + \beta \left(\sum_{j=1}^n K_{SP,ij}(\mathbf{x})e_j\right) \left|\sum_{j=1}^n K_{SP,ij}(\mathbf{x})e_j\right|^{\frac{q}{p}-1},$$

to compute the time derivative of the sliding surface, considering $\frac{d}{dt}|f(t)| = \frac{f(t)\dot{f}(t)}{|f(t)|}$, as in the following:

$$\begin{aligned} \dot{s}_i &= \ddot{e}_i + \beta \left(\sum_{j=1}^n \dot{K}_{SP,ij}(\mathbf{x})e_j + \sum_{j=1}^n K_{SP,ij}(\mathbf{x})\dot{e}_j \right) \left| \sum_{j=1}^n K_{SP,ij}(\mathbf{x})e_j \right|^{\frac{q}{p}-1} \\ &+ \beta \left(\frac{q}{p} - 1 \right) \left(\sum_{j=1}^n \dot{K}_{SP,ij}(\mathbf{x})e_j \right. \\ &\left. + \sum_{j=1}^n K_{SP,ij}(\mathbf{x})\dot{e}_j \right) \frac{\sum_{j=1}^n K_{SP,ij}(\mathbf{x})e_j}{\left| \sum_{j=1}^n K_{SP,ij}(\mathbf{x})e_j \right|} \left| \sum_{j=1}^n K_{SP,ij}(\mathbf{x})e_j \right|^{\frac{q}{p}-2} \left(\sum_{j=1}^n K_{SP,ij}(\mathbf{x})e_j \right). \end{aligned} \quad (36)$$

Replacing $\frac{\sum_{j=1}^n K_{SP,ij}(\mathbf{x})e_j}{\left| \sum_{j=1}^n K_{SP,ij}(\mathbf{x})e_j \right|} = \text{sign}(\sum_{j=1}^n K_{SP,ij}(\mathbf{x})e_j)$, Eq. (36) is rewritten as

$$\begin{aligned} \dot{s}_i &= \ddot{e}_i + \beta \left(\sum_{j=1}^n \dot{K}_{SP,ij}(\mathbf{x})e_j + \sum_{j=1}^n K_{SP,ij}(\mathbf{x})\dot{e}_j \right) \left| \sum_{j=1}^n K_{SP,ij}(\mathbf{x})e_j \right|^{\frac{q}{p}-1} \\ &+ \beta \left(\frac{q}{p} - 1 \right) \left(\sum_{j=1}^n \dot{K}_{SP,ij}(\mathbf{x})e_j \right. \\ &\left. + \sum_{j=1}^n K_{SP,ij}(\mathbf{x})\dot{e}_j \right) \left[\text{sign} \left(\sum_{j=1}^n K_{SP,ij}(\mathbf{x})e_j \right) \right]^2 \left| \sum_{j=1}^n K_{SP,ij}(\mathbf{x})e_j \right|^{\frac{q}{p}-1}. \end{aligned} \quad (37)$$

Notice that $[\text{sign}(\cdot)]^2 = 1$, then Eq. (37) is simplified as

$$\dot{s}_i = \ddot{e}_i + \beta \frac{q}{p} \left(\sum_{j=1}^n \dot{K}_{SP,ij}(\mathbf{x})e_j + \sum_{j=1}^n K_{SP,ij}(\mathbf{x})\dot{e}_j \right) \left| \sum_{j=1}^n K_{SP,ij}(\mathbf{x})e_j \right|^{\frac{q}{p}-1}.$$

References

- [1] X. Yu and O. Kaynak, "Sliding-mode control with soft computing: A survey," *IEEE transactions on industrial electronics*, vol. 56, pp. 3275-3285, 2009.
- [2] S. T. Venkataraman and S. Gulati, "Control of nonlinear systems using terminal sliding modes," 1993.
- [3] M. Zhihong and X. H. Yu, "Terminal sliding mode control of MIMO linear systems," *IEEE Transactions on Circuits and Systems I: Fundamental Theory and Applications*, vol. 44, pp. 1065-1070, 1997.
- [4] S. Yu, X. Yu, B. Shirinzadeh, and Z. Man, "Continuous finite-time control for robotic manipulators with terminal sliding mode," *Automatica*, vol. 41, pp. 1957-1964, 2005.

Nekoo, Saeed Rafee, JoséÁngel Acosta, and Anibal Ollero. "Combination of terminal sliding mode and finite-time state-dependent Riccati equation: Flapping-wing flying robot control." *Proceedings of the Institution of Mechanical Engineers, Part I: Journal of Systems and Control Engineering* (2022): 09596518221138627.

DOI: <https://doi.org/10.1177/09596518221138627>

- [5] Y. Feng, X. Yu, and F. Han, "On nonsingular terminal sliding-mode control of nonlinear systems," *Automatica*, vol. 49, pp. 1715-1722, 2013.
- [6] M. H. Korayem, R. Shiri, S. R. Nekoo, and Z. Fazilati, "Non-singular terminal sliding mode control design for wheeled mobile manipulator," *Industrial Robot: An International Journal*, vol. 44, pp. 501-511, 2017.
- [7] M. Boukattaya, N. Mezghani, and T. Damak, "Adaptive nonsingular fast terminal sliding-mode control for the tracking problem of uncertain dynamical systems," *ISA transactions*, vol. 77, pp. 1-19, 2018.
- [8] Y. Wang, S. Jiang, B. Chen, and H. Wu, "A new continuous fractional-order nonsingular terminal sliding mode control for cable-driven manipulators," *Advances in Engineering software*, vol. 119, pp. 21-29, 2018.
- [9] A. T. Vo and H.-J. Kang, "An adaptive terminal sliding mode control for robot manipulators with non-singular terminal sliding surface variables," *IEEE Access*, vol. 7, pp. 8701-8712, 2018.
- [10] G. Wang and Q. Xu, "Adaptive terminal sliding mode control for motion tracking of a micropositioning system," *Asian Journal of Control*, 2018.
- [11] J.-J. Xiong and G.-B. Zhang, "Global fast dynamic terminal sliding mode control for a quadrotor UAV," *ISA transactions*, vol. 66, pp. 233-240, 2017.
- [12] R. Shiri, S. Rafee Nekoo, M. Habibnejad Korayem, and S. Kazemi, "Finite-time nonsingular terminal sliding mode control: A time setting approach," *Proceedings of the Institution of Mechanical Engineers, Part I: Journal of Systems and Control Engineering*, vol. 233, pp. 1392-1412, 2019.
- [13] S. R. Nekoo, "Tutorial and review on the state-dependent Riccati equation," *Journal of Applied Nonlinear Dynamics*, vol. 8, pp. 109-166, 2019.
- [14] S. R. Nekoo, J. R. Acosta, and A. Ollero, "Quaternion-based state-dependent differential Riccati equation for quadrotor drones: Regulation control problem in aerobatic flight," *Robotica*, 2022.
- [15] N. S. Tripathy, I. N. Kar, and K. Paul, "Finite-time robust control of robot manipulator: a SDDRE based approach," in *Proceedings of the 2015 Conference on Advances In Robotics*, Goa, India, 2015, p. 56.
- [16] M. H. Korayem and S. R. Nekoo, "State-dependent differential Riccati equation to track control of time-varying systems with state and control nonlinearities," *ISA Transactions*, vol. 57, pp. 117-135, 2015.
- [17] A. Heydari and S. N. Balakrishnan, "Approximate closed-form solutions to finite-horizon optimal control of nonlinear systems," in *American Control Conference*, Fairmont Queen Elizabeth, Montréal, Canada, 2012, pp. 2657-2662.
- [18] A. Heydari and S. N. Balakrishnan, "Fixed-final-time optimal tracking control of input-affine nonlinear systems," *Neurocomputing*, vol. 129, pp. 528-539, 2014.
- [19] J.-W. Jung, S.-Y. Park, S.-W. Kim, Y. Eun, and Y.-K. Chang, "Hardware-in-the-loop simulations of spacecraft attitude synchronization using the state-dependent Riccati equation technique," *Advances in Space Research*, vol. 51, pp. 434-449, 2013.
- [20] B. Etkin, *Dynamics of atmospheric flight*: Courier Corporation, 2012.
- [21] T. I. Fossen, "Mathematical models for control of aircraft and satellites," *Department of Engineering Cybernetics Norwegian University of Science and Technology*, pp. 54-58, 2011.
- [22] G. K. Taylor and A. L. R. Thomas, "Animal flight dynamics II. Longitudinal stability in flapping flight," *Journal of theoretical biology*, vol. 214, pp. 351-370, 2002.
- [23] B. W. Tobalske, "Biomechanics of bird flight," *Journal of Experimental Biology*, vol. 210, pp. 3135-3146, 2007.
- [24] X. Deng, L. Schenato, W. C. Wu, and S. S. Sastry, "Flapping flight for biomimetic robotic insects: Part I-system modeling," *IEEE Transactions on Robotics*, vol. 22, pp. 776-788, 2006.
- [25] M. F. Platzer, K. D. Jones, J. Young, and J. C. S. Lai, "Flapping wing aerodynamics: Progress and challenges," *AIAA Journal*, vol. 46, pp. 2136-2149, 2008.
- [26] J. E. Bluman and C.-K. Kang, "Balancing the efficiency and stability of the coupled dynamics and aerodynamics of a flapping flyer," in *AIAA Modeling and Simulation Technologies Conference*, 2016, p. 4009.
- [27] B. Cheng and X. Deng, "Translational and rotational damping of flapping flight and its dynamics and stability at hovering," *IEEE Transactions on Robotics*, vol. 27, pp. 849-864, 2011.
- [28] B. Cheng, S. N. Fry, Q. Huang, W. B. Dickson, M. H. Dickinson, and X. Deng, "Turning dynamics and passive damping in flapping flight," in *2009 IEEE International Conference on Robotics and Automation*, 2009, pp. 1889-1896.
- [29] P. Chirarattananon, Y. Chen, E. F. Helbling, K. Y. Ma, R. Cheng, and R. J. Wood, "Dynamics and flight control of a flapping-wing robotic insect in the presence of wind gusts," *Interface Focus*, vol. 7, p. 20160080, 2017.

Nekoo, Saeed Rafee, JoséÁngel Acosta, and Anibal Ollero. "Combination of terminal sliding mode and finite-time state-dependent Riccati equation: Flapping-wing flying robot control." *Proceedings of the Institution of Mechanical Engineers, Part I: Journal of Systems and Control Engineering* (2022): 09596518221138627.

DOI: <https://doi.org/10.1177/09596518221138627>

- [30] D. B. Doman, M. W. Oppenheimer, and D. O. Sigthorsson, "Wingbeat shape modulation for flapping-wing micro-air-vehicle control during hover," *Journal of guidance, control, and dynamics*, vol. 33, pp. 724-739, 2010.
- [31] W. Shyy, H. Aono, S. K. Chimakurthi, P. Trizila, C.-K. Kang, C. E. S. Cesnik, *et al.*, "Recent progress in flapping wing aerodynamics and aeroelasticity," *Progress in Aerospace Sciences*, vol. 46, pp. 284-327, 2010.
- [32] J. P. Whitney and R. J. Wood, "Aeromechanics of passive rotation in flapping flight," *Journal of fluid mechanics*, vol. 660, p. 197, 2010.
- [33] B. E. Wissa, K. O. Elshafei, and A. A. El-Badawy, "Lyapunov-based control and trajectory tracking of a 6-DOF flapping wing micro aerial vehicle," *Nonlinear Dynamics*, pp. 1-20, 2020.
- [34] S. F. Armanini, M. Karásek, C. C. de Visser, G. de Croon, and M. Mulder, "Flight testing and preliminary analysis for global system identification of ornithopter dynamics using on-board and off-board data," in *AIAA Atmospheric Flight Mechanics Conference*, 2017, p. 1634.
- [35] A. M. Hassan and H. E. Taha, "Differential-geometric-control formulation of flapping flight multi-body dynamics," *Journal of Nonlinear Science*, vol. 29, pp. 1379-1417, 2019.
- [36] A. Bakhtiari, S. Ehtemadi H., and A. Maghsoudpour, "Modeling and control of a flapping wing robot," *Proceedings of the Institution of Mechanical Engineers, Part K: Journal of Multi-body Dynamics*, vol. 233, pp. 174-181, 2019.
- [37] M. A. Amini, M. Ayati, and M. Mahjoob, "A simplified model, dynamic analysis and force estimation for a large-scale ornithopter in forward flight based on flight data," *Journal of Bionic Engineering*, pp. 1-20, 2020.
- [38] C. Ding, "Dynamic performances of a bird-like flapping wing robot under randomly uncertain disturbances," *PloS one*, vol. 15, p. e0232202, 2020.
- [39] A. G. Eguíluz, J. P. Rodríguez-Gómez, J. L. Paneque, P. Grau, J. R. M. de Dios, and A. Ollero, "Towards flapping wing robot visual perception: Opportunities and challenges," in *2019 Workshop on Research, Education and Development of Unmanned Aerial Systems (RED UAS)*, 2019, pp. 335-343.
- [40] G. He, T. Su, T. Jia, L. Zhao, and Q. Zhao, "Dynamics analysis and control of a bird scale underactuated flapping-wing vehicle," *IEEE Transactions on Control Systems Technology*, 2019.
- [41] S. R. Nekoo, "Digital implementation of a continuous-time nonlinear optimal controller: An experimental study with real-time computations," *ISA transactions*, vol. 101, pp. 346-357, 2020.
- [42] M. H. Korayem and S. R. Nekoo, "Finite-time state-dependent Riccati equation for time-varying nonaffine systems: Rigid and flexible joint manipulator control," *ISA Transactions*, vol. 54, pp. 125-144, 2015.
- [43] S. R. Nekoo, J. R. Acosta, G. Heredia, and A. Ollero, "A PD-type state-dependent Riccati equation with iterative learning augmentation for mechanical systems," *IEEE/CAA Journal of Automatica Sinica*, 2022.
- [44] B. Geranmehr and S. R. Nekoo, "Precision control of double-gimbal magnetically suspended control moment gyros," in *3rd RSI International Conference on Robotics and Mechatronics*, Tehran, Iran, 2015, pp. 31-36.
- [45] M. H. Korayem and S. R. Nekoo, "Controller design of cooperative manipulators using state-dependent Riccati equation," *Robotica*, vol. 36, pp. 484-515, 2018.
- [46] M. H. Korayem, S. R. Nekoo, and A. H. Korayem, "Finite time SDRE control design for mobile robots with differential wheels," *Journal of Mechanical Science and Technology*, vol. 30, pp. 4353-4361, 2016.
- [47] Z. Xu, W. Huang, Z. Li, L. Hu, and P. Lu, "Nonlinear nonsingular fast terminal sliding mode control using deep deterministic policy gradient," *Applied Sciences*, vol. 11, p. 4685, 2021.
- [48] J.-J. E. Slotine and W. Li, *Applied nonlinear control* vol. 199: Prentice-Hall Englewood Cliffs, NJ, 1991.
- [49] X. Yu, Y. Feng, and Z. Man, "Terminal sliding mode control-An overview," *IEEE Open Journal of the Industrial Electronics Society*, 2020.
- [50] M. Li, Z. Zuo, H. Liu, C. Liu, and B. Zhu, "Adaptive fault tolerant control for trajectory tracking of a quadrotor helicopter," *Transactions of the Institute of Measurement and Control*, vol. 40, pp. 3560-3569, 2018.